

AD-A076 153 ARMY ELECTRONICS RESEARCH AND DEVELOPMENT COMMAND WS--ETC F/G 14/2
HELICOPTER REMOTE WIND SENSOR SYSTEM DESCRIPTION.(U)
SEP 79 D H DICKSON , C M SONNENSCHN
UNCLASSIFIED ERADCOM/ASL-TR-0040 NL

1 OF 1
AD
A076153



END
DATE
FILMED
11-79
DDC

12 LEVEL II

AD

ASL-TR-0040

Reports Control Symbol
OSD 1366

AD A 076153

HELICOPTER REMOTE WIND SENSOR SYSTEM DESCRIPTION

SEPTEMBER 1979

By

David H. Dickson

Atmospheric Sciences Laboratory
White Sands Missile Range, NM 88002

Charles M. Sonnenschein

Equipment Development Laboratories
Raytheon Company
Sudbury, MA 01776

DDC
RECEIVED
NOV 6 1979
B

DDC FILE COPY

Approved for public release; distribution unlimited



US Army Electronics Research and Development Command
ATMOSPHERIC SCIENCES LABORATORY
White Sands Missile Range, NM 88002

79 11 05 117

NOTICES

Disclaimers

The findings in this report are not to be construed as an official Department of the Army position, unless so designated by other authorized documents.

The citation of trade names and names of manufacturers in this report is not to be construed as official Government endorsement or approval of commercial products or services referenced herein.

Disposition

Destroy this report when it is no longer needed. Do not return it to the originator.

REPORT DOCUMENTATION PAGE		READ INSTRUCTIONS BEFORE COMPLETING FORM
1. REPORT NUMBER ERADCO ON/ASL-TR-0040	2. GOVT ACCESSION NO. 9 Research and development	3. RECIPIENT'S CATALOG NUMBER
4. TITLE (and Subtitle) HELICOPTER REMOTE WIND SENSOR SYSTEM DESCRIPTION	5. TYPE OF REPORT & PERIOD COVERED R&D Technical Report	6. PERFORMING ORG. REPORT NUMBER
7. AUTHOR(s) David H. Dickson Charles M. Sonnenschein	8. CONTRACT OR GRANT NUMBER(s)	
9. PERFORMING ORGANIZATION NAME AND ADDRESS Atmospheric Sciences Laboratory White Sands Missile Range, NM 88002	10. PROGRAM ELEMENT, PROJECT, TASK AREA & WORK UNIT NUMBERS DA Task No 1162117AH71	
11. CONTROLLING OFFICE NAME AND ADDRESS US Army Electronics Research and Development Command Adelphi, MD 20783	12. REPORT DATE September 1979	13. NUMBER OF PAGES 45
14. MONITORING AGENCY NAME & ADDRESS (if different from Controlling Office) 1257	15. SECURITY CLASS. (of this report) UNCLASSIFIED	15a. DECLASSIFICATION/DOWNGRADING SCHEDULE
16. DISTRIBUTION STATEMENT (of this Report) Approved for public release: distribution unlimited.		
17. DISTRIBUTION STATEMENT (of the abstract entered in Block 20, if different from Report)		
18. SUPPLEMENTARY NOTES *Equipment Development Laboratories Raytheon Company Sudbury, MA 01776		
19. KEY WORDS (Continue on reverse side if necessary and identify by block number) Lasers Laser Doppler velocimeter Helicopter Remote wind sensing		
20. ABSTRACT (Continue on reverse side if necessary and identify by block number) The helicopter remote wind sensor (HRWS) is an application of a laser Doppler velocimeter. This system description describes the HRWS fabricated by Raytheon Company for the US Army Atmospheric Sciences Laboratory. The HRWS was designed to measure wind fields in an aircraft turbulent environment. The operational emphasis is to augment an attack helicopter's fire control system. This CO ₂ laser heterodyne system		

410 663

45

20. ABSTRACT (CONT)

remotely measures three dimensional winds from 1 to 33 meters in front of the sensor. The HRWS was mounted in an external pod compatible with AH-1, AAH and UH-1 wing stores or a fixed wing aircraft equipped with standard wing shackles. The HRWS theory, functions, and subsystem are discussed. Data from flight and ground testing will be presented in a later report.

CONTENTS

LIST OF FIGURES	4
LIST OF TABLES	5
INTRODUCTION	7
Doppler Theory	7
CONICAL SCANNING SYSTEM - THEORETICAL BACKGROUND	8
SYSTEM DESCRIPTION	10
Laser	10
Heterodyne Optics	11
Beam Expander	11
Range Scanner	11
Conical Scanners	12
Receiver	12
Frequency Tracker	13
Pod	14
Controls	15
Integrated Sensor System	15
CONCLUSIONS	15
FIGURES	16
TABLES	38

ACCESSION for	
NTIS	White Section <input checked="" type="checkbox"/>
DDC	Buff Section <input type="checkbox"/>
UNANNOUNCED	<input type="checkbox"/>
JUSTIFICATION _____	
BY _____	
DISTRIBUTION/AVAILABILITY CODES	
Dist.	AVAIL. and/or SPECIAL
A	

FIGURES

1.	Artist's concept of helicopter remote wind sensor (HRWS)	16
2.	Helicopter remote wind sensor (pod open)	17
3.	Laser Doppler velocimeter transmission and reception	18
4.	Laser Doppler velocity measurement	19
5.	Illustration of optical heterodyning	19
6.	Sample ground wind velocity distribution from a coaxial nonscanning system	20
7.	System geometry	20
8.	Block design of helicopter remote wind sensor	21
9.	CO ₂ laser (scale [in photo] is 12 inches)	22
10.	Back-reflection optical diagram	23
11.	Range scanning	24
12.	Time function of range scanner	24
13.	Angle scanner optical layout	25
14.	Detector characteristics	26
15.	Detector characteristics	27
16.	Detector characteristics	28
17.	Remote wind sensor frequency tracker	29
18.	Frequency counter	29
19.	Minimum SNR vs frequency	30
20.	Helicopter pod	31
21.	HRWS control panel	32
22.	System interconnection	33
23.	Helicopter carried remote wind sensor with corners open	34
24.	Helicopter carried remote wind sensor	35
25.	Mounted helicopter remote wind sensor	36
26.	Sensor and tape recorder	37

TABLES

1.	Beam Expander Specifications	38
2.	Wedge Specifications	40
3.	Measured Detector Parameters	41
4.	Tracker Parameters	42
5.	Frequency Measurements	43
6.	Controls for HRWS	44

INTRODUCTION

This report describes the helicopter remote wind sensor built by Raytheon Company for the US Army Atmospheric Sciences Laboratory. The system was designed to fly on an AH-1 helicopter (attack helicopter) to improve the accuracy of free flight armament, e.g., 2.75-in. rockets, by measuring the atmospheric flow field along the rocket path. Measurements were made of the wind field from ranges of 1 to 32 m in front of the sensor and every 2 degrees around a 17-degree half-angle cone. These data allow the calculation of the three dimensional flow field vector as a function of range. The sensor system is located in a pod that can be suspended below the stub wing of the AH-1 helicopter. An artist's concept is shown in figure 1, and the actual system mounted on a UH-1 helicopter (utility helicopter) (used for test purposes) is shown in figure 2.

This report is a system description only and as such does not present analyses, conclusions, or recommendations typically contained in technical test reports.

Doppler Theory

Operation of a laser Doppler velocimeter may be understood with the aid of figure 3. A laser beam is transmitted through an interferometer which passes most of the energy to the target and diverts a small amount to the detector as shown in figure 3A. The transmitted beam is usually passed through a telescope to the target, which in the present case consists of aerosols naturally suspended in the atmosphere. Some of the transmitted energy is backscattered by the target particles and enters the detector by the path shown in figure 3B. This returning energy has been shifted in frequency by an amount proportional to the component of particle velocity parallel to the direction of propagation V_{\parallel} , according to the Doppler principle. Figure 4 shows the geometry of the laser system and target velocity vector relationship. Only V_{\parallel} contributes to the Doppler shift.

Two beams fall on the detector at two different frequencies (figure 5): a reference beam at the optical frequency f_o with a power of a few milliwatts and the smaller power signal beam at the new frequency $f_o + f_d$, where f_d is the Doppler shift frequency. When these beams are superimposed, the combination contains energy at the difference of these frequencies.

The difference is the Doppler frequency and is related to the target velocity. A sample spectrum in figure 6 shows the intensity as a function of frequency for a laser velocimeter system signal. There is a peak at 0.7 MHz corresponding to a velocity of about 3.35 m/s for $f_o = \frac{C}{\lambda} = 2.83 \times 10^{13}$ Hz. C = speed of light; λ = wavelength.

CONICAL SCANNING SYSTEM - THEORETICAL BACKGROUND

The use of a coaxial heterodyne laser system to obtain a component of the velocity vector of the atmosphere has been described in the previous paragraphs. A conical scan can also be performed with the beam from the system to measure all three vector components. This technique is described in this portion of the report.

The system geometry is illustrated in figure 7. The cone has an axis \hat{r} which lies in the x-z plane at an angle θ with the z-axis. The half-apex angle of the cone is $\delta/2$. If at time, $t = 0$, the propagation vector \vec{K} is in the x-z plane, then

$$\vec{K} = |K| \left[\cos \frac{\delta}{2} \hat{r} + \sin \frac{\delta}{2} \cos \omega t \hat{p}_x + \sin \frac{\delta}{2} \sin \omega t \hat{p}_y \right], \quad (1)$$

where ω is the scanning frequency. P_x and P_y are as defined in figure 7, with P_y normal to P_x . For an arbitrary velocity vector,

$$\vec{V} = V_x \hat{i} + V_y \hat{j} + V_z \hat{k} \quad (2)$$

The Doppler frequency shift is proportional to the dot product of \vec{K} and \vec{V} ,

$$f_D = - \frac{\vec{K} \cdot \vec{V}}{\pi}. \quad (3)$$

Substituting equations (1) and (2) into equation (3),

$$\begin{aligned} f_D = - \frac{|K|}{\pi} & \left[\cos \frac{\delta}{2} (V_x \sin \theta + V_z \cos \theta) \right. \\ & + \cos \omega t \sin \frac{\delta}{2} (V_x \cos \theta - V_z \sin \theta) \\ & \left. + \sin \omega t \sin \frac{\delta}{2} V_y \right]. \quad (4) \end{aligned}$$

The Doppler shift consists of two parts: a DC term f_{DC} equal to $- |K|/\pi \cos \delta/2 (V_x \sin \theta + V_z \cos \theta)$ and a time varying term f_{AC}

equal to $-\frac{|K|}{\pi} \cos \omega t \sin \frac{\delta}{2} (V_x \cos \theta - V_z \sin \theta) + \sin \omega t \sin \frac{\delta}{2} V_y$. Since the angles θ and δ are known, the three velocity components can be determined in the following fashion. At time, $t = \frac{\pi}{2\omega}$, the magnitude of the time varying term is proportional to the velocity component in the y-direction. Thus

$$V_y = - \frac{\pi}{|K| \sin \frac{\delta}{2}} f_{AC} \Big|_{t = \frac{\pi}{2\omega}} \quad (5)$$

The x and z components can be found by the DC term and the AC term at time, $t = 0$.

$$f_{DC} (t = 0) = - \frac{|K|}{\pi} \cos \frac{\delta}{2} (V_x \sin \theta + V_z \cos \theta), \quad (6)$$

$$f_{AC} (t = 0) = - \frac{|K|}{\pi} \sin \frac{\delta}{2} (V_z \cos \theta - V_x \sin \theta). \quad (7)$$

Solving equations (6) and (7) simultaneously,

$$V_x = \frac{\pi \left[f_{DC} \sin \theta \sin \frac{\delta}{2} - f_{AC}(t = 0) \cos \theta \cos \frac{\delta}{2} \right]}{|K| \cos \frac{\delta}{2} \sin \frac{\delta}{2} (\sin^2 \theta - \cos^2 \theta)}, \quad (8)$$

$$V_z = \frac{\pi \left[f_{DC} \cos \theta \sin \frac{\delta}{2} - f_{AC}(t = 0) \sin \theta \cos \frac{\delta}{2} \right]}{|K| \cos \frac{\delta}{2} \sin \frac{\delta}{2} (\sin^2 \theta - \cos^2 \theta)}. \quad (9)$$

The principle of least squares is applied by fitting a rectified biased sinusoidal function to the HRWS data. Subsequently, the V_x , V_y , V_z wind components are determined from the coefficients obtained by the fitting process. The equations used are contained in the HRWS flight test report (to be published).

SYSTEM DESCRIPTION

A CO₂ laser heterodyne system has been constructed and mounted in a pod compatible with an AH-1 or a UH-1 helicopter. A block diagram of the system is shown in figure 8. The HRWS can be subdivided into three subsystems: the transmitter, the scanners, and the processor. The transmitter consists of a CO₂ laser and appropriate beam combining optics for heterodyne operation. Two scanners are employed: one scans in range and the other produces a conical scan. The processor includes the detector and its associated biasing network, frequency tracker, and a tape recorder.

The following paragraphs describe the individual components.

Laser

Other studies have determined that a 5-W laser would provide sufficient power to reliably measure helicopter flow fields, a previously developed Raytheon Company 5-W air-cooled laser with low weight and size and an extremely high degree of ruggedness and reliability was selected. This laser was designed as a result of numerous system analyses, which indicated a need for a 5-W lightweight, rugged, air-cooled laser, specifically designed for operation in a field environment. Among the primary design goals for such a device were:

1. All-metal/ceramic laser tube, replacing the fragile glass tube of laboratory lasers
2. Direct air-cooling of the laser tube, eliminating liquid coolants
3. Stable lightweight laser frame.

Raytheon has built and tested a laser meeting these requirements and has successfully flown it as part of a system.¹

The laser frame consists of a magnesium alloy box within which four invar rods, connecting the two end plates, are contained. An all-ceramic alumina plasma tube is terminated by zinc selenide Brewster angle windows. The mirrors are contained in spherical mounts in the end plates and are prealigned and then permanently fixed in place. The clamp-on fins for cooling are of anodized aluminum. The laser is cooled by room air directed through the laser frame. A photograph of the CO₂ laser is shown in figure 9.

¹Contract 33615-73-C-1321, CO₂ Laser Heterodyne Sensor

Tests on this laser conducted during several programs have been impressive, with sustained output power as high as 6 W. The laser has been tested to determine its output power as a function of tube wall temperature, with no ill effects even though no cooling was supplied to the laser for periods in excess of 30 min.

Several design features are incorporated to achieve adequate laser lifetime. A gas reservoir is contained in the central portion surrounding the cathode. The laser uses a split discharge configuration with anodes on both ends and air cooling fins applied to both sections of the tube. A separate, high voltage power supply is used to power each half of the discharge tube. The units chosen for this application are modular, current-regulated supplies and contain an automatic starting circuit to initiate the laser discharge.

Laser lifetime in excess of 200 hr has been obtained with this laser. The lifetime is usually determined by decomposition of the gas; and when the power decreases significantly, the laser may be refilled through a valve on the laser tube incorporated into the design.

Heterodyne Optics

The heterodyne optics consist of a combination of beam splitters and polarizing elements that generate the local oscillator (LO) and the transmitter beams and recombine the collected signal with the LO. Measurements of the detector indicate that LO beams of approximately 1 to 2 mW provide the maximum signal-to-noise ratio (SNR). The reflectivity of the beam splitters has been selected to generate an LO beam of this value. The remainder of the energy is transmitted into a beam expander (described in the next paragraph). After the beam expander collects the scattered energy, the heterodyne optics combine LO and signal and direct this superposition toward the detector (described in paragraph entitled "Receiver"). The polarizing elements of the heterodyne optics assure proper polarization of all beams.

Beam Expander

Table 1 lists the specifications of the beam expander. The optical design resulted in a Galilean telescope with an input negative singlet and an output doublet. Figure 10 shows a back-reflection optical diagram for the surface reflection properties.

Range Scanner

Range scanning is accomplished by translating the input lens of the beam expander described in the previous paragraph. Motion of the input lens translates the location of the focused laser beam as shown

in figure 11. If the input lens were scanned linearly with time, too much time would be spent at closer ranges. Therefore, a nonlinear drive function is electronically generated, which gives the scan as a function of time as shown in figure 12. The results shown in this figure were obtained experimentally from the assembled HRWS.

The range scanner is controlled by a three-position switch. In the off position, the beam becomes collimated (focuses at infinity); in the manual position, a potentiometer permits the operator to focus the beam at any range. The automatic switch position generates a range scan in which the beam varies its focus from 1 to 33 m in approximately 1 s. Under all conditions, a voltage proportional to the range of the focus is available for display and recording.

Conical Scanners

The conical scan is generated by rotating a wedge counterclockwise relative to direction of propagation about the optical axis. The wedge specifications are given in table 2, and the configuration is shown in figure 13. The wedge is driven by a motor whose speed is variable from 0 to 2300 r/min. To insure adequate bearing lifetime, the delivered system was limited to a speed of 1300 r/min. The motor speed is adjusted by a potentiometer and can be displayed on the control panel. As the motor speed decreases below a few hundred revolutions per minute, the laser beam is automatically blocked for safety reasons, preventing propagation into the atmosphere. Although the beam blocking mechanism can be overridden for alignment procedures, a caution light on the control panel warns the operator. In addition to measurements of the motor speed, signals are available every 2.8 degrees of rotation to indicate the angular beam position.

Receiver

The receiver consists of a 10.6 μ m detector and the associated bias circuit and amplifiers. The requirements of high quantum efficiency and good frequency response dictated the use of a mercury-cadmium-telluride (HgCdTe) detector. The detector is mounted in a dewar which holds liquid nitrogen for a period of at least 6 hr. The electronic circuitry of the receiver was designed to minimize loss of SNR.

The present performance of commercially available metal dewars is very good. With capacities of 0.25 l, the hold time is 6 to 8 hr. Such a dewar fits into a 6-in. cube. Windows are easily dismantled if they need to be replaced. For future operational systems, other cooling techniques are available.

The function of the bias circuit is to provide a voltage supply to the detector and to provide the proper matching between the receiver pre-amplifier and the detector. A prime requirement in designing this

circuit is to protect the detector from excess voltages or currents that can result from removal of the LO, too high LO power, or loss of coolant in the detector dewar.

A Honeywell HgCdTe detector was purchased, and its parameters were measured. The results of this measurement are given in table 3, and graphs of detector characteristics are shown in figures 14, 15, and 16.

Frequency Tracker

This portion describes the frequency tracker and counter built for the HRWS. The equipment is capable of measuring fixed frequency or sinusoidally frequency modulated inputs. The measured characteristics for the tracker are listed in table 4.

Figure 17 is a block diagram of the frequency tracker. The input band is translated up to a center frequency of f_o by mixing the input with the output of a voltage-controlled oscillator (VCO). The signal is then limited and fed through a frequency discriminator centered near f_o . In tracking operations, the discriminator drives an integrator, the output of which drives the VCO. With the tracking loop closed, the sum of the input and VCO frequencies is constant.

Since the discriminator frequency range is much smaller than the input band, acquisition circuits are included to initially center the translated input in the discriminator band. A ramp generator sweeps the VCO over its range until the acquisition detector detects the presence of a signal in the discriminator band; at this time the loop is closed and the input tracked. The acquisition detector will revert to the search mode when the amplitude of the bandpass filter output is insufficient for tracking.

For automatic calibration purposes the input signal is periodically replaced by the output of a crystal oscillator. The readout circuit makes use of measurements made during this calibration interval to automatically correct for drift in the discriminator and integrator.

The frequency counter (figure 18) counts the positive zero crossings of the VCO during a $160\mu\text{s}$ period once each angle clock pulse. The sample gate generator provides this accurately timed counter gate along with a pulse immediately after it to clock the output storage register.

The calibration gate generator periodically generates a gate which turns on the 5-MHz calibration oscillator. After waiting for a period of time for the tracker to acquire the 5-MHz calibration signal and for the VCO to settle, a single $160\mu\text{s}$ sample of the VCO frequency is taken by the calibration counter. The calibration counter output is then subtracted from all frequency readings to automatically correct for discriminator center frequency drift.

A single-bit output is provided which declares data invalid during calibration and under loss of track.

The results of laboratory tests on the frequency tracker for the helicopter wind sensor are summarized. Test results include minimum SNR, frequency accuracy, dynamic range, and acquisition time. Measurements of the SNR (referenced to a 1-MHz noise bandwidth ± 1) required to track are shown in figure 19. The probability of tracking (P_T) is the fraction of the time which the tracker stays in its tracking mode. Due to the extremely sharp nature of the threshold levels at the high end of the band, these measurements were made only to 9 MHz. At 10 MHz, a 17-dB input SNR produced nearly 100 percent tracking.

Measurements of the accuracy of the counter output were made at two signal levels and three frequencies. The results are listed in table 5. Each output measurement shown is the average of five samples of the counter output. The worst error with self-calibration employed is 17.5 kHz.

A 2-MHz input signal was varied in level from -48 dBm to +2 dBm; a 25-kHz shift in measured frequency occurred over this 50 dB of input range. The tracker was then disabled and the harmonic content of the signal was examined with a spectrum analyzer. At the +2 dBm input level, the worst harmonic level generated in the preamp/translator circuitry appeared at a frequency 4 MHz above the translated fundamental. Its level was 24 dB below the translated fundamental.

To obtain the maximum sensitivity possible, the sweep excursion has been increased to 12 MHz; the VCO now sweeps from 36 to 48 MHz. The time required to sweep this range is 240 μ s, and the time required to dump the integrator is 15 μ s. The worst case acquisition time is, therefore, 255 μ s.

Pod

The integration of any system into the compact package required to fit into an AH-1 helicopter is expensive and time-consuming. Additionally, packaging will relate to only a given installation and will require modifications for alternative vehicles. Therefore, it was decided that for this phase of the program the most cost-effective and timely choice would be to build an airworthy pod, similar to the rocket pods currently used on the AH-1, to enclose the system. The mounting brackets from an existing rocket pod were used, and the remainder of the pod was fabricated. Figure 20 shows a picture of the pod before the sensor was installed.

Controls

The sensor in the pod is operated from a control panel (figure 21) in the helicopter. All operations on the system are performed from the control panel except filling the detector with liquid nitrogen, which was done during aircraft preflight. The control panel also has a number of diagnostic capabilities which may be used by maintenance personnel. The controls and their functions are shown in table 6.

The data may be obtained from the data panel as shown in figure 22. These data are suitable for recording on a tape recorder such as the Ampex CP-100 which was used during the flight tests.

Integrated Sensor System

Several photographs of the assembled HRWS system are presented. Figure 23 shows the system with the pod doors open so that details of the components are visible. Figure 24 shows a closed pod. Figure 25 shows the system attached to a UH-1 helicopter during tests. The tape recorder, used for data collection, is clearly visible in figure 26.

CONCLUSIONS

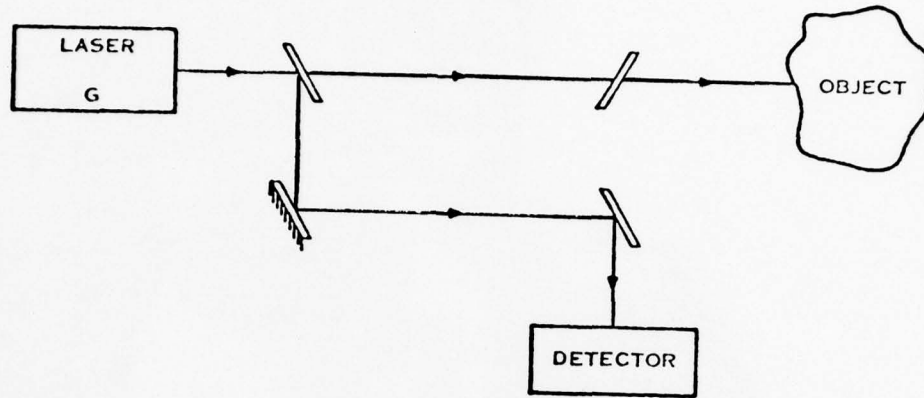
A CO₂ laser Doppler velocimeter has been successfully miniaturized and packaged for airborne operations. The HRWS has successfully functioned as designed in flight tests. The HRWS will measure wind speed and direction and potentially can augment a fire control system for attack helicopters. The HRWS can readily be used as a diagnostic tool for aircraft wind field investigation and as a ground-based wind sensor to measure atmosphere winds.



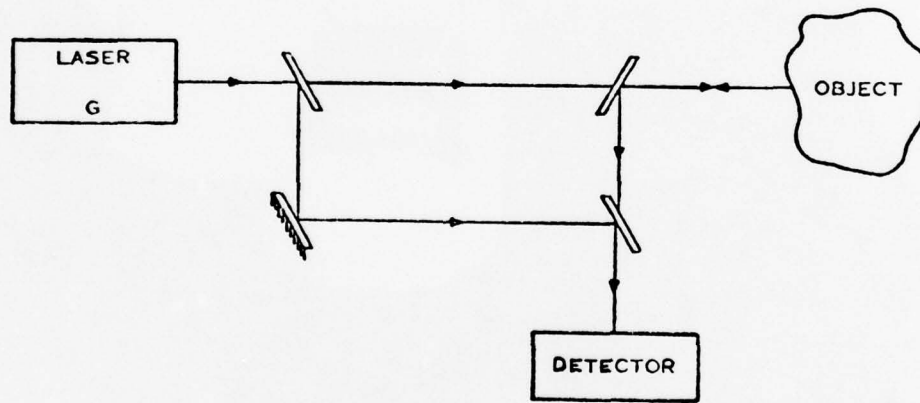
Figure 1. Artist's concept of helicopter remote wind sensor (HRWS).



Figure 2. Helicopter remote wind sensor (pod open).



A. Paths of transmitted beam.



B. Paths of transmitted and received beams.

Figure 3. Laser Doppler velocimeter transmission and reception.

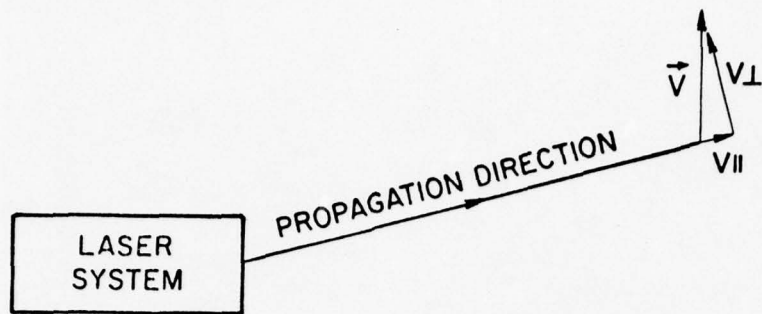


Figure 4. Laser Doppler velocity measurement.

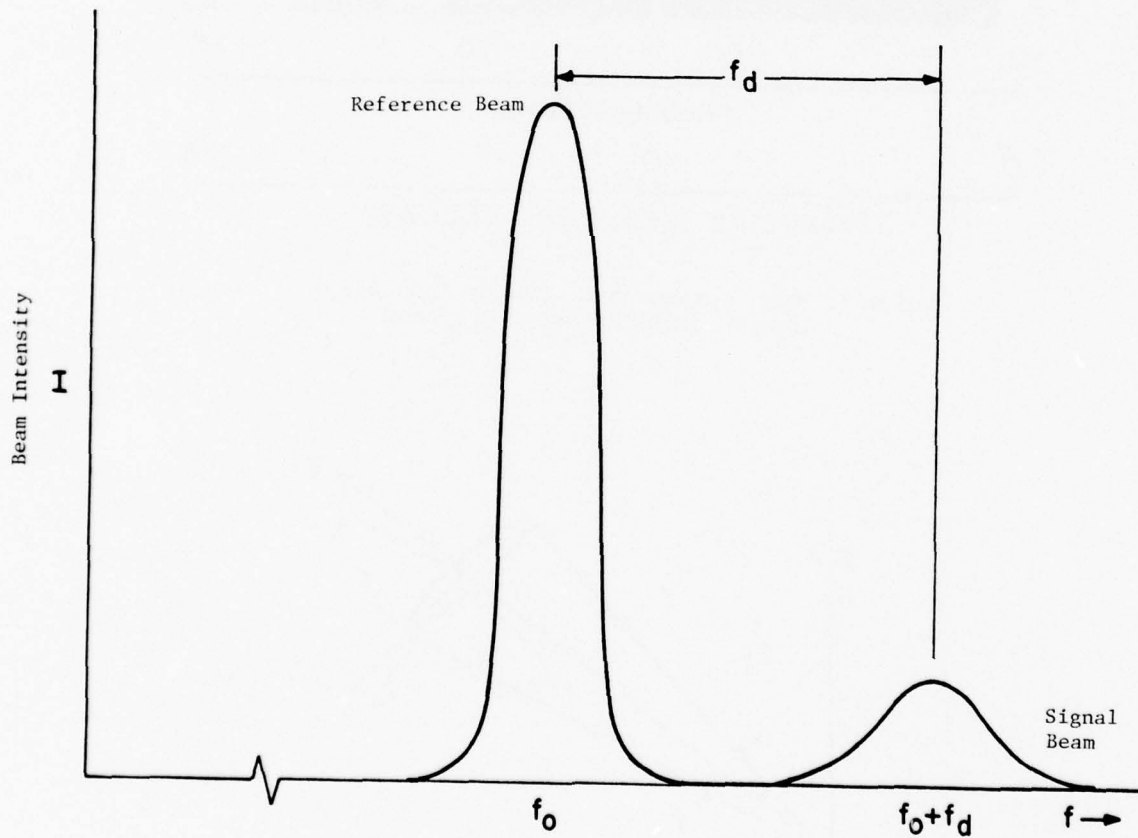


Figure 5. Illustration of optical heterodyning.

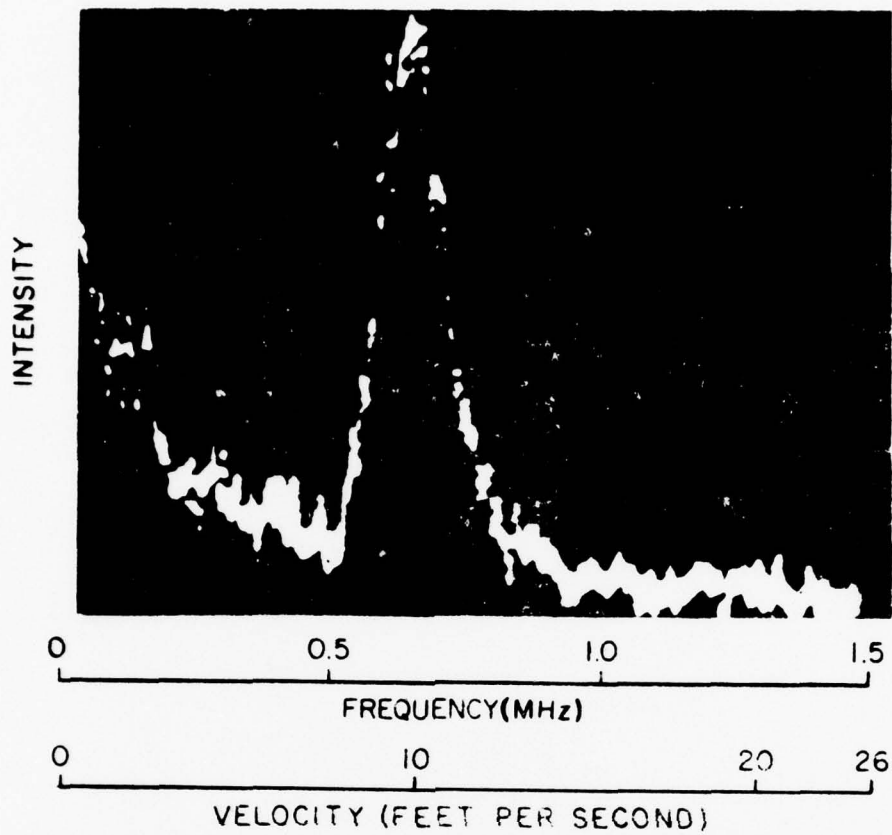


Figure 6. Sample ground wind velocity distribution from a coaxial non-scanning system.

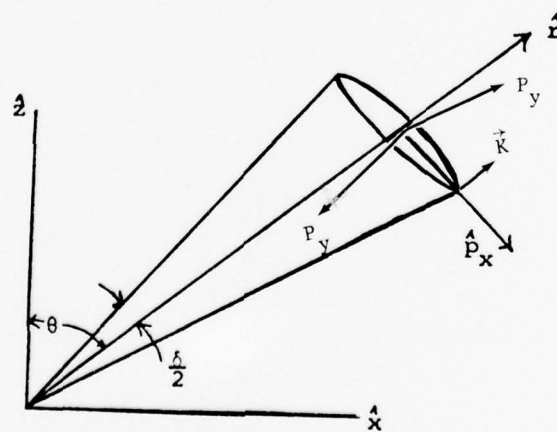


Figure 7. System geometry.

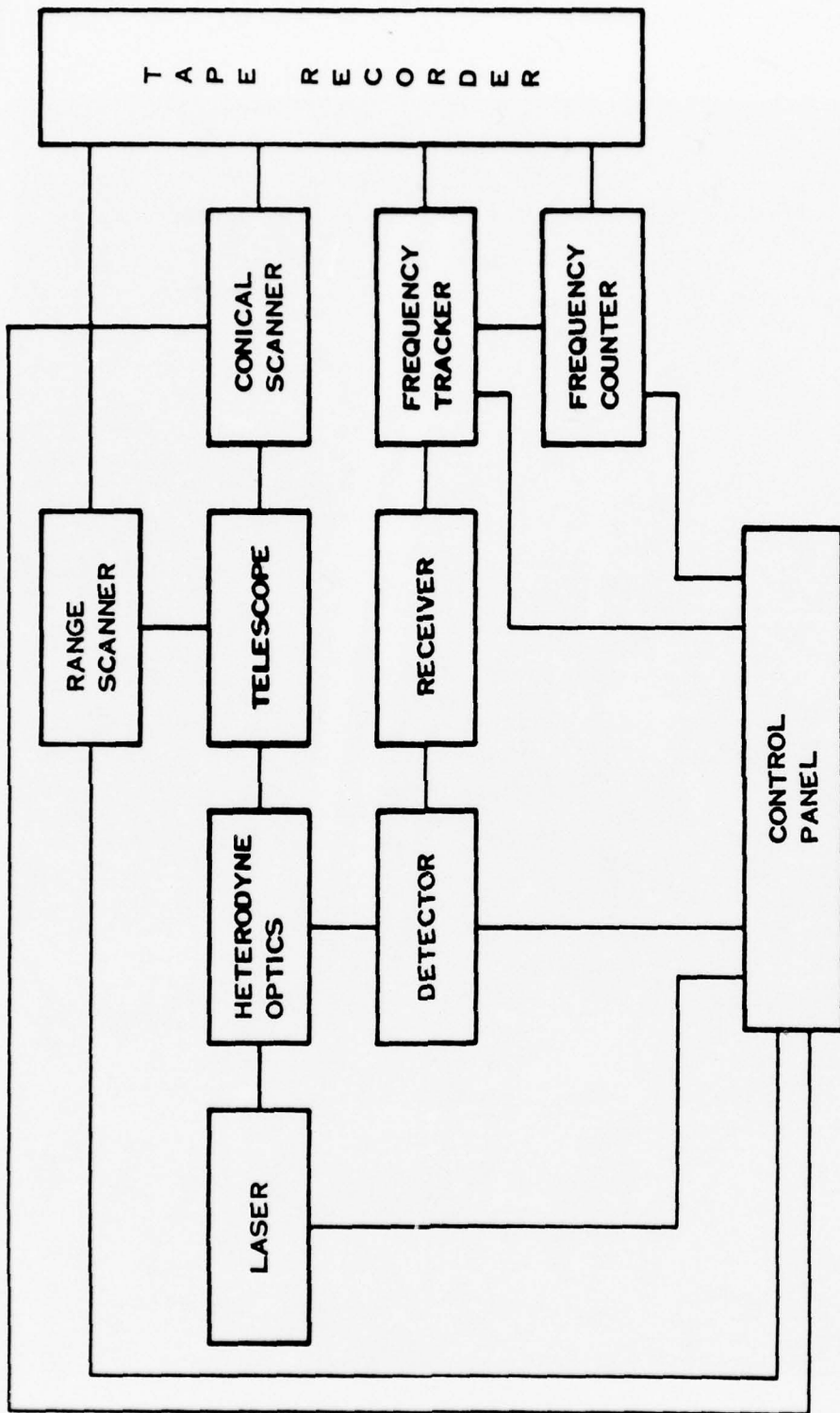


Figure 8. Block design of helicopter remote wind sensor.

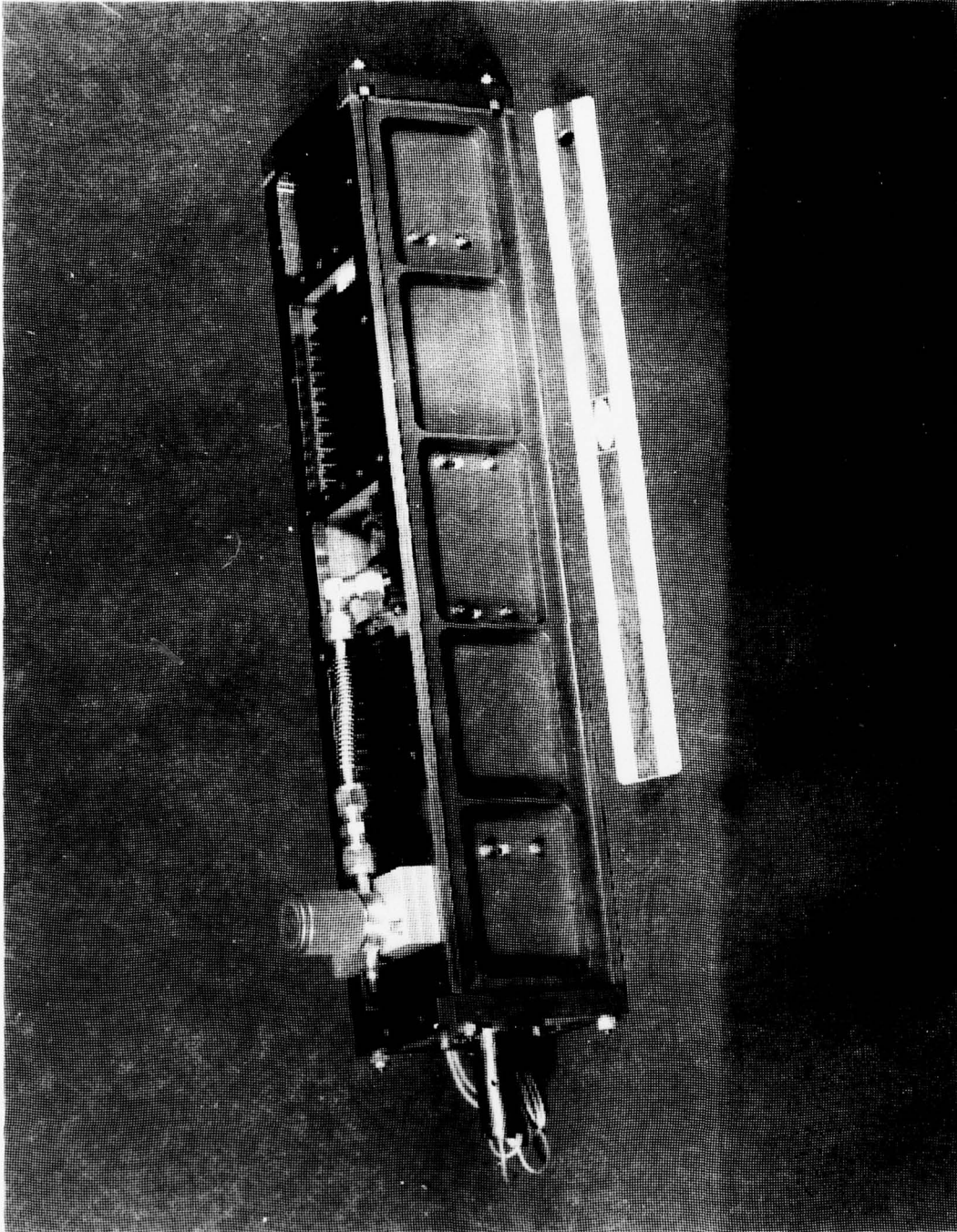


Figure 9. CO₂ laser (scale [in photo] is 12 inches).

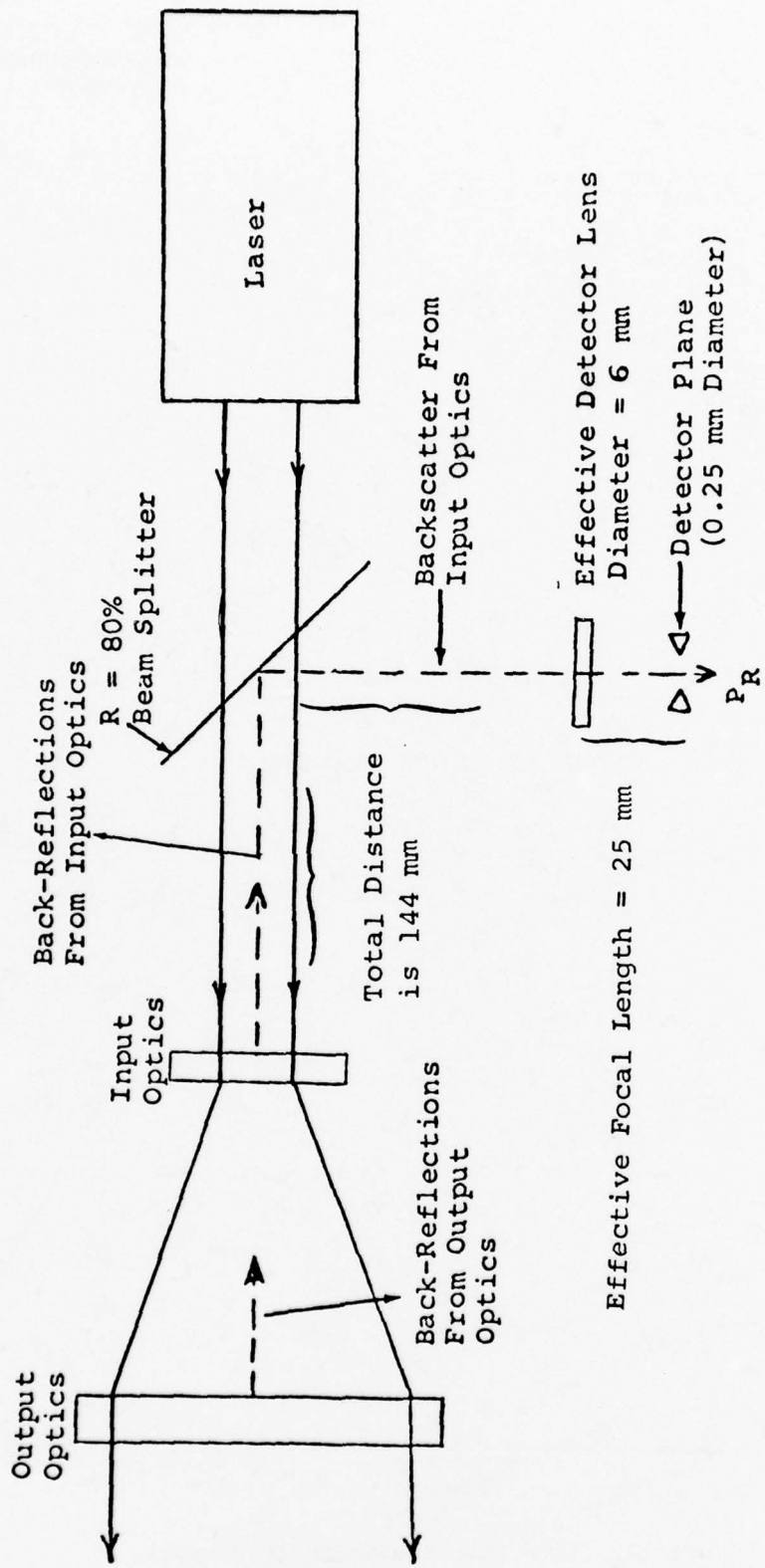


Figure 10. Back-reflection optical diagram.

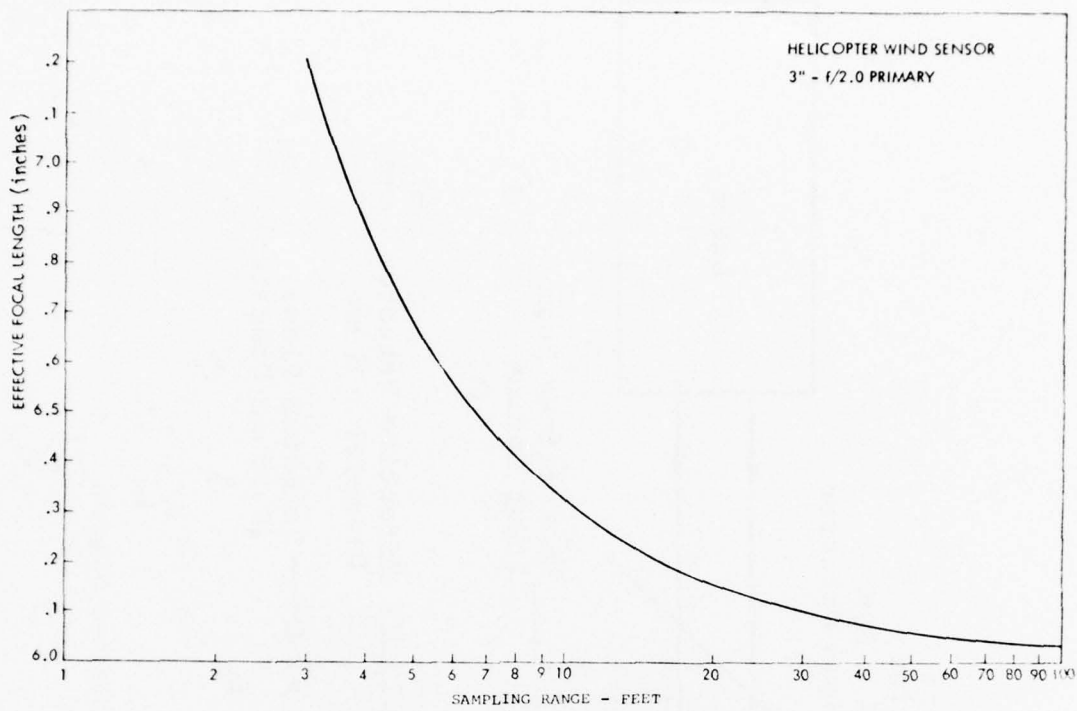


Figure 11. Range scanning.

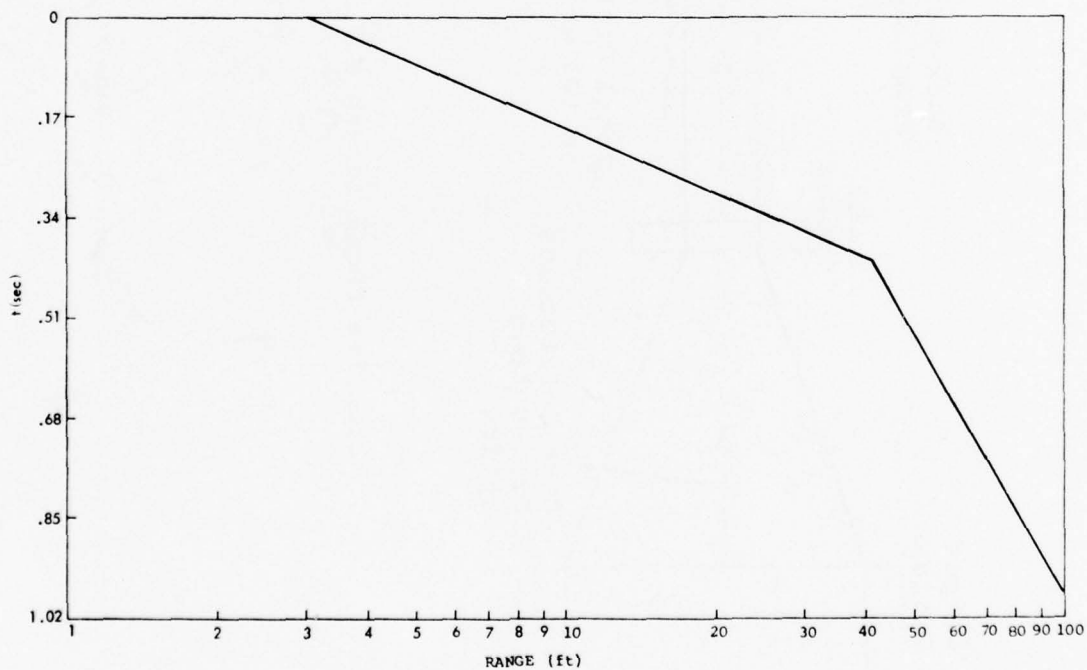


Figure 12. Time function of range scanner.

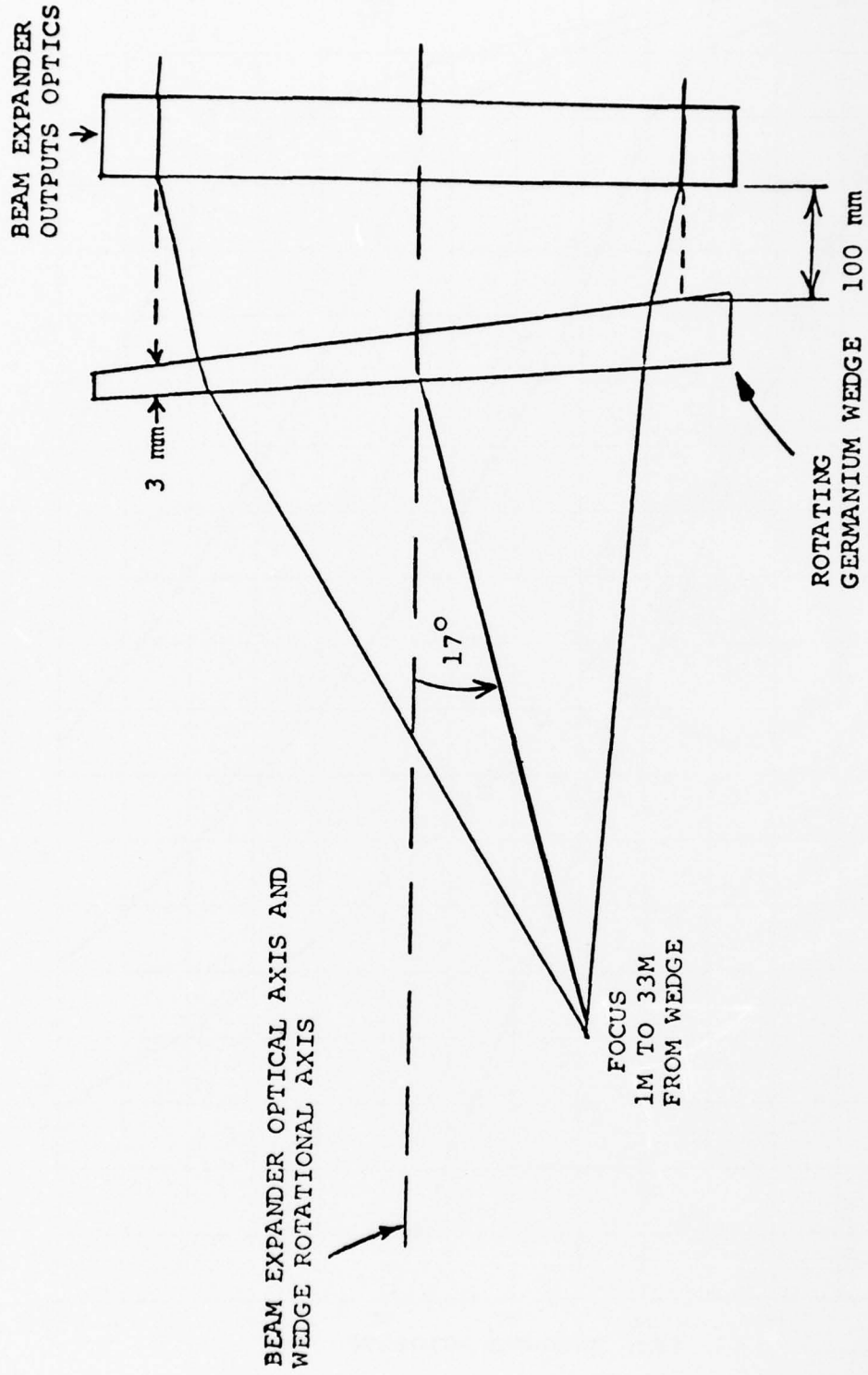


Figure 13. Angle scanner optical layout.

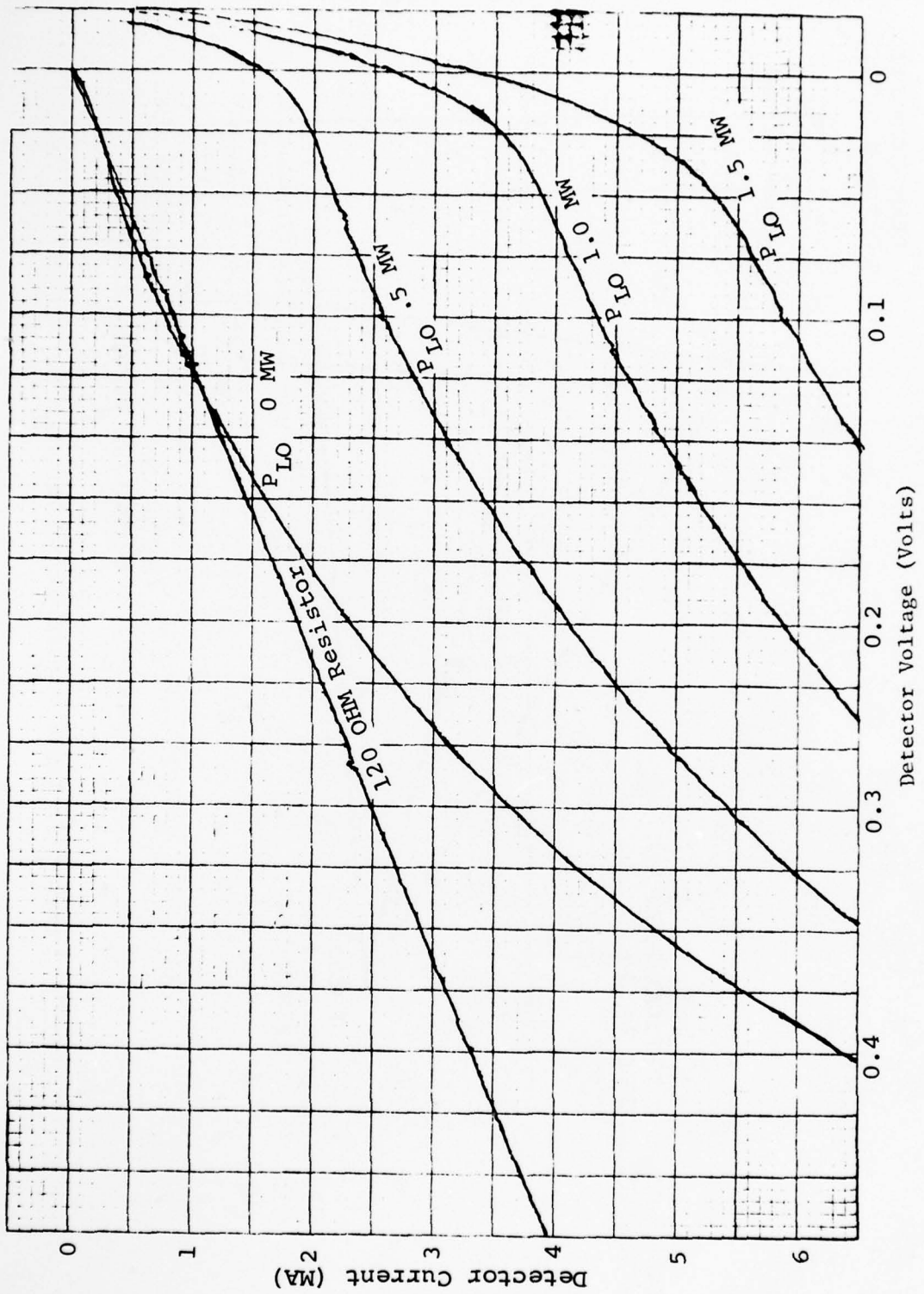


Figure 14. Detector characteristics.

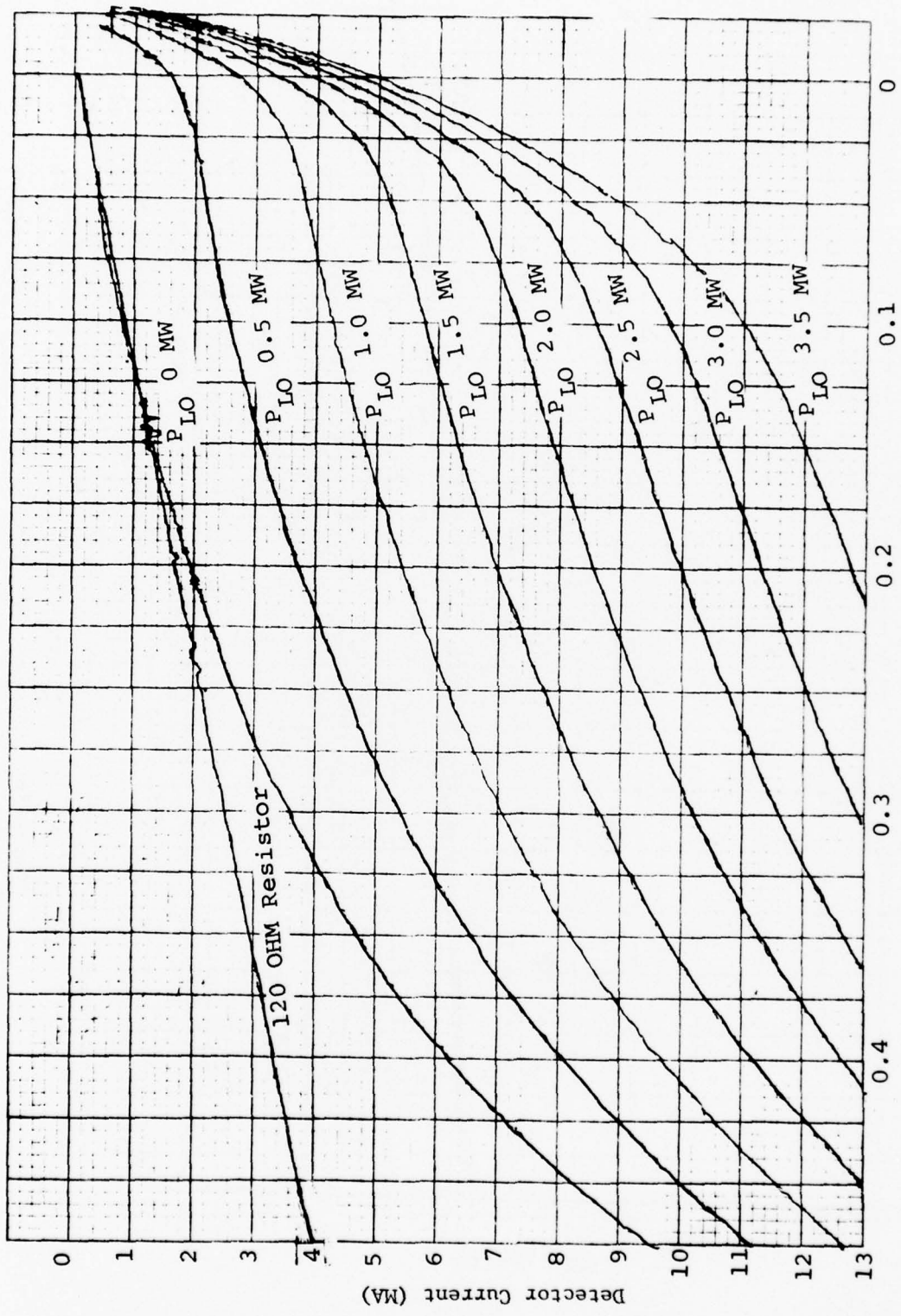


Figure 15. Detector characteristics.

B.W. 300 KHz

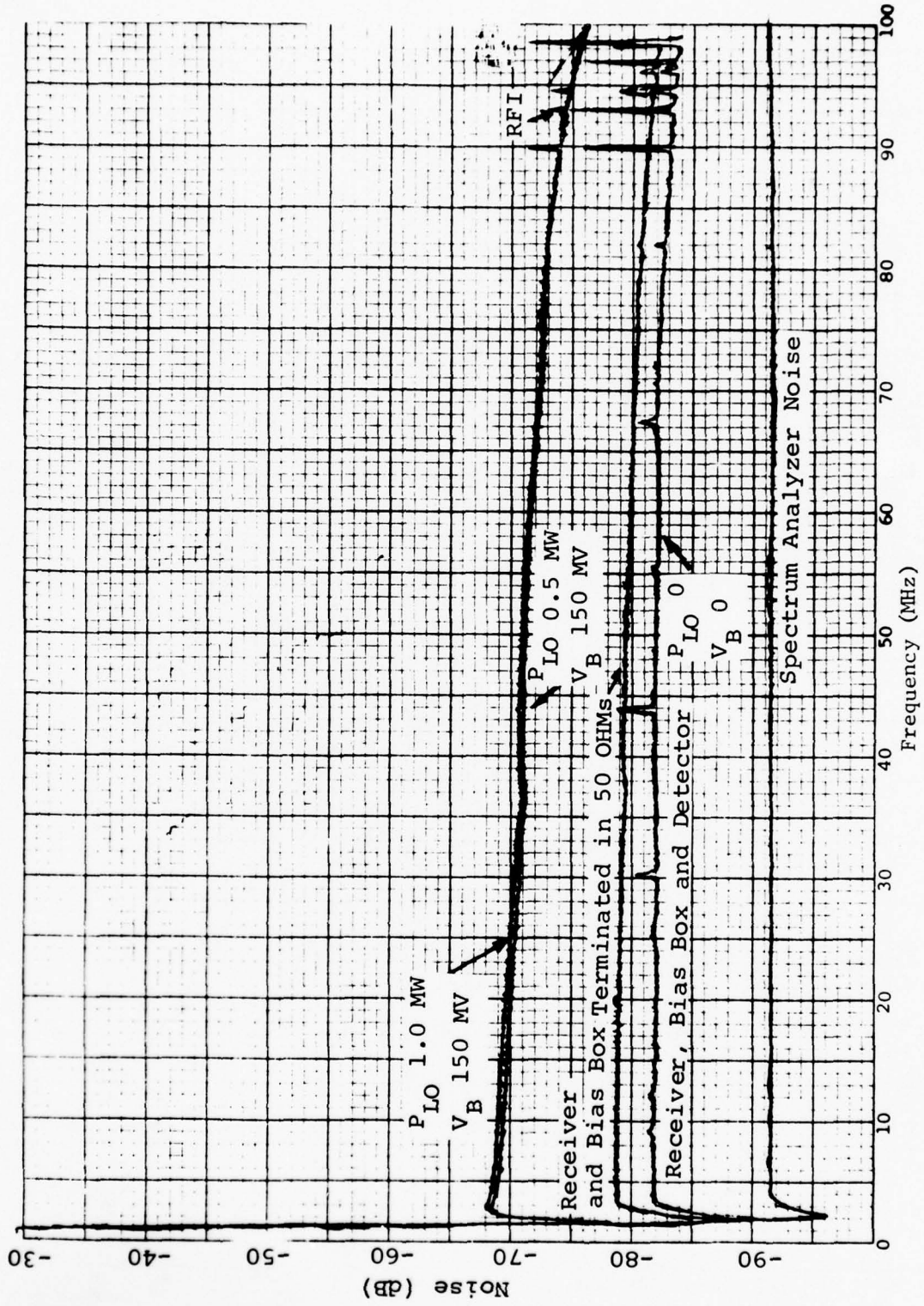


Figure 16. Detector characteristics.

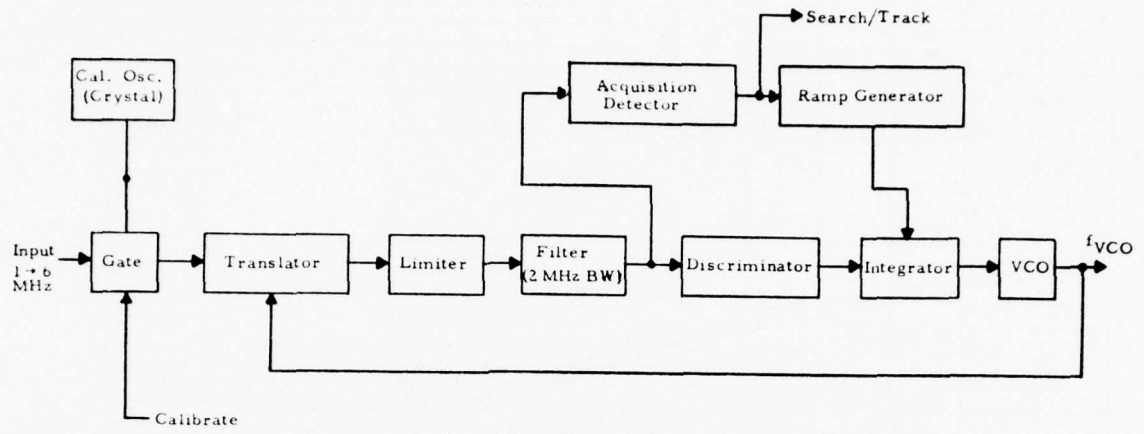


Figure 17. Remote wind sensor frequency tracker.

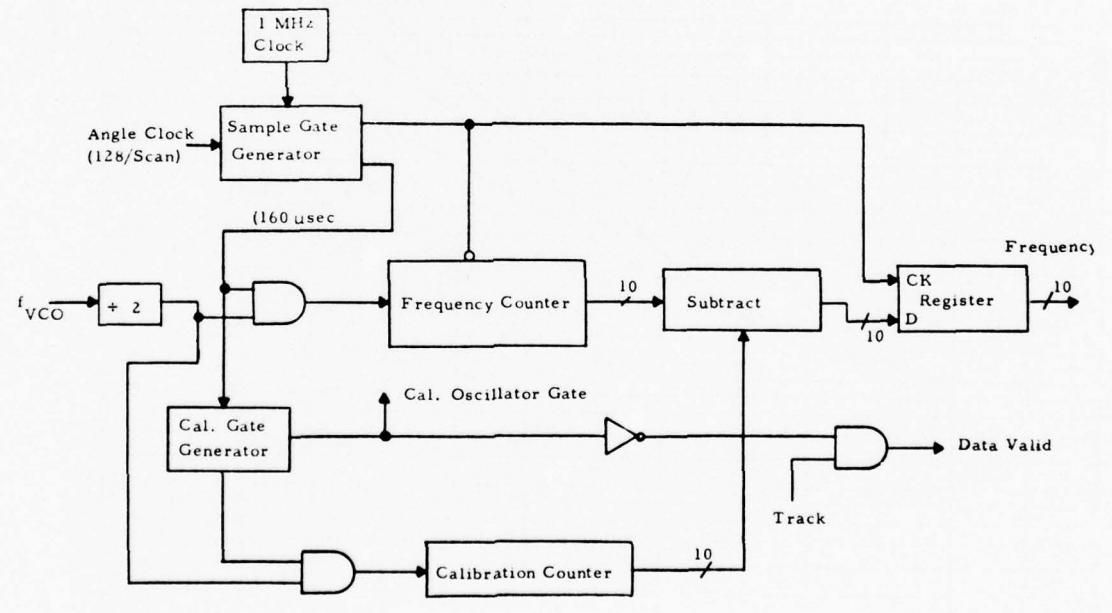
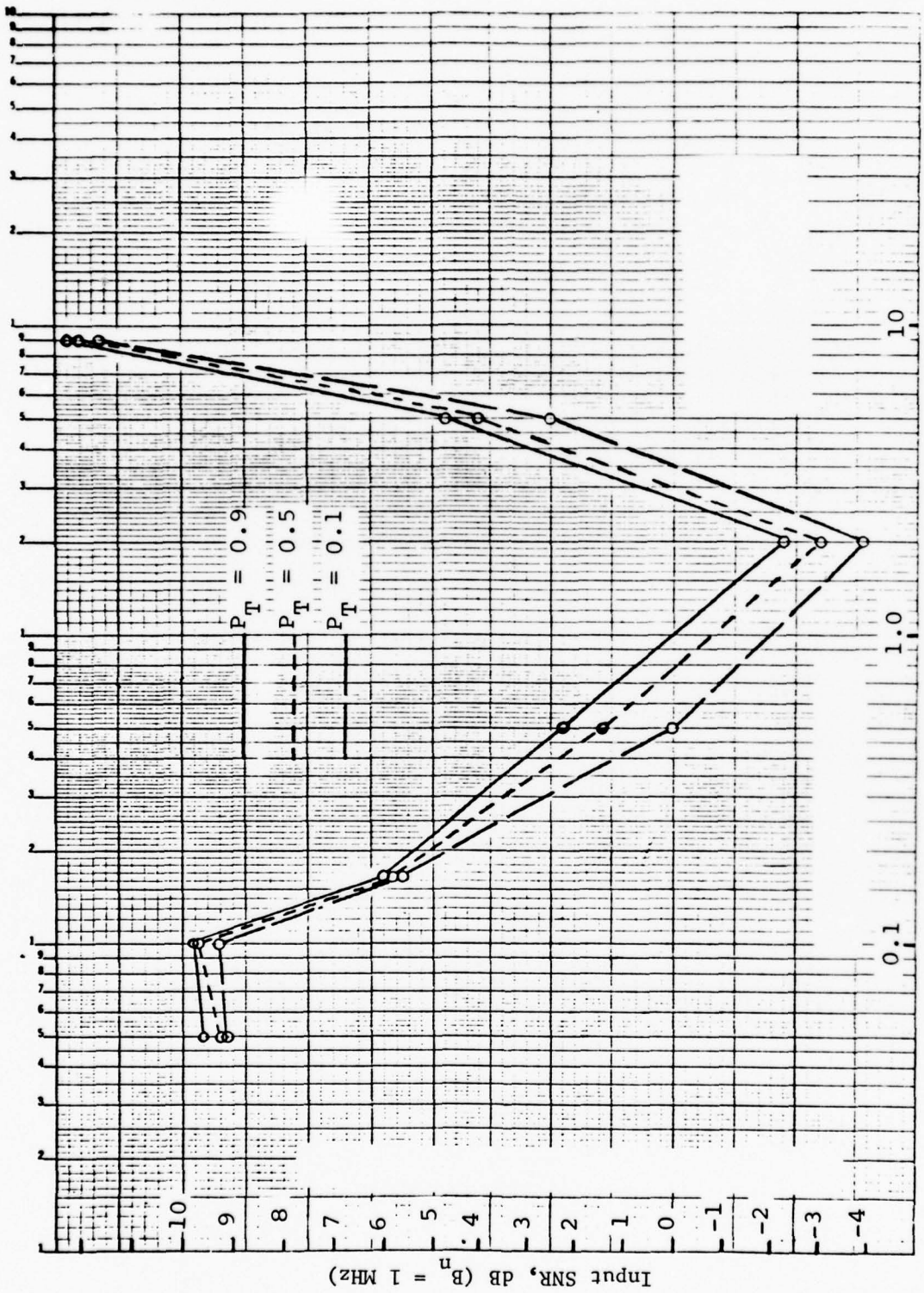


Figure 18. Frequency counter.



Frequency, MHz

Figure 19. Minimum SNR vs frequency.

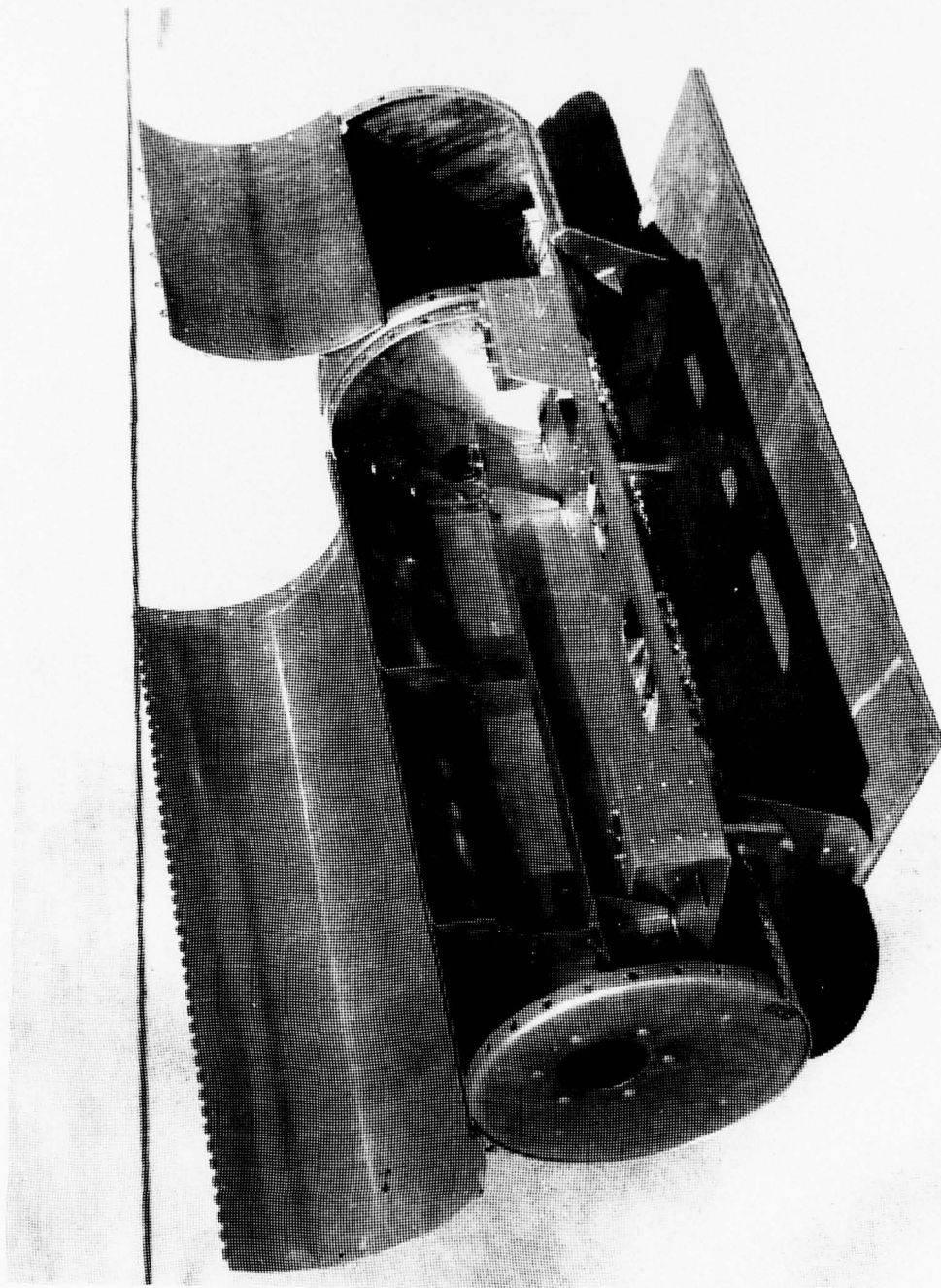


Figure 20. Helicopter pod.

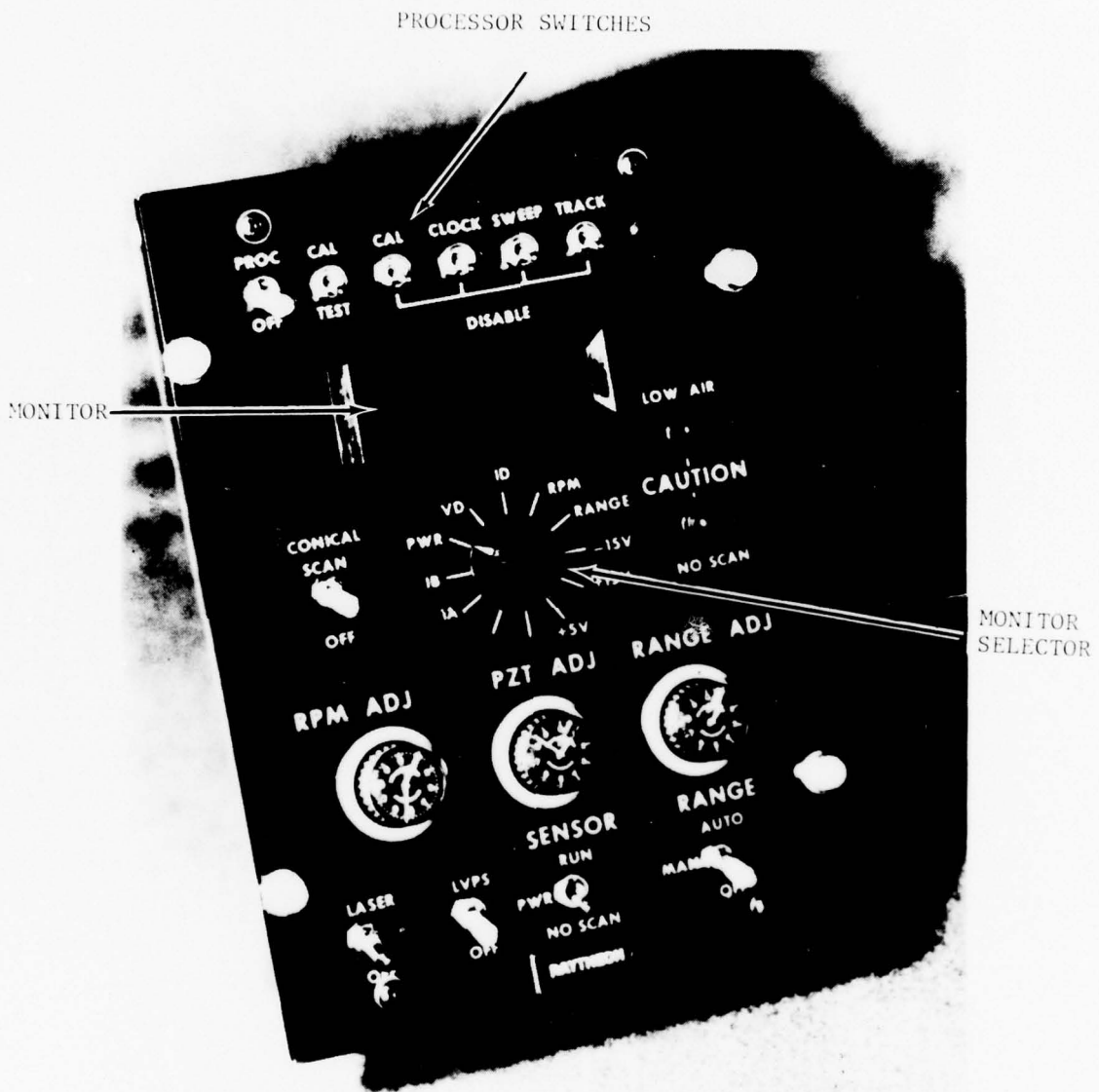


Figure 21. HRWS control panel.

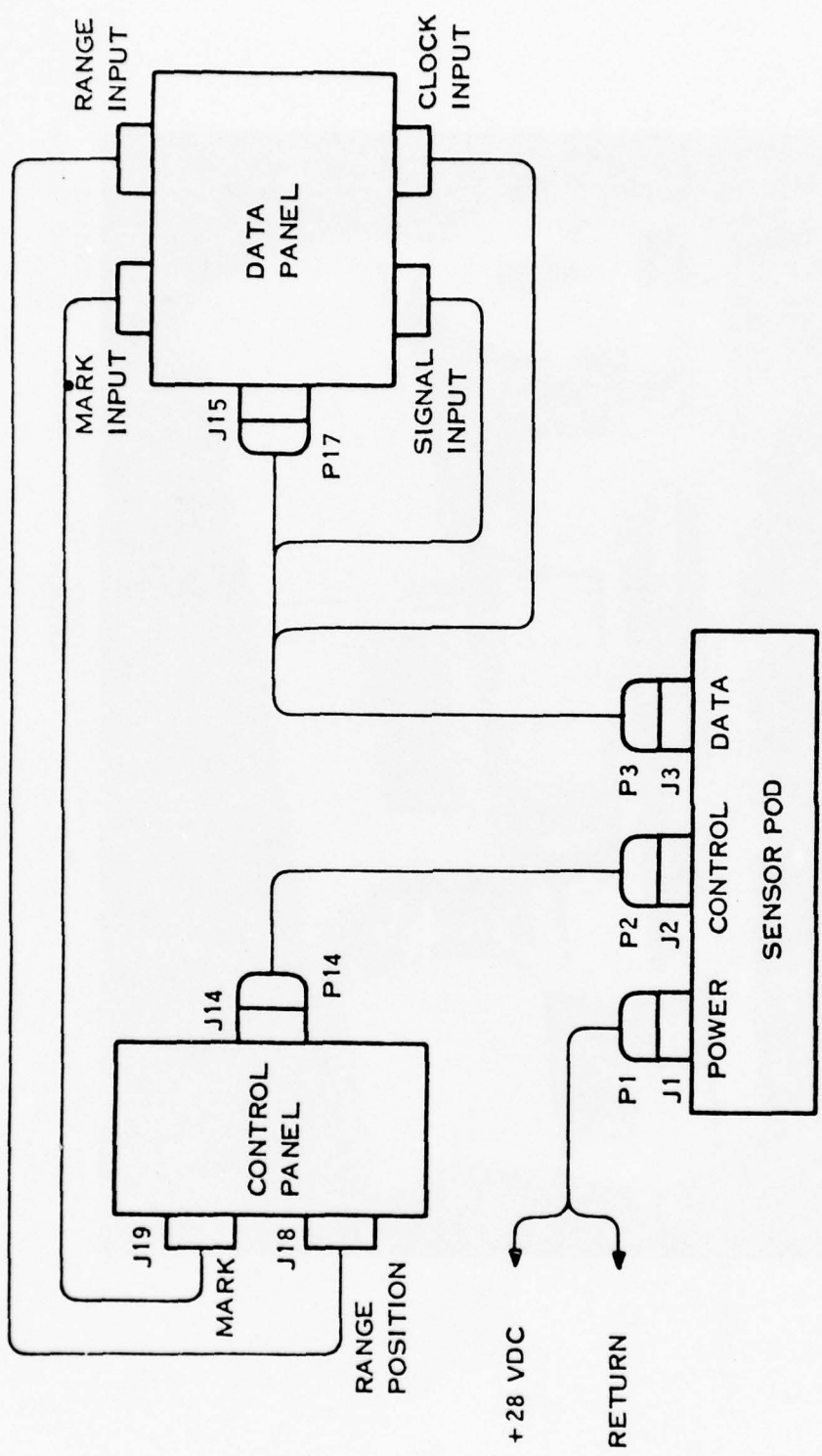


Figure 22. System interconnection.

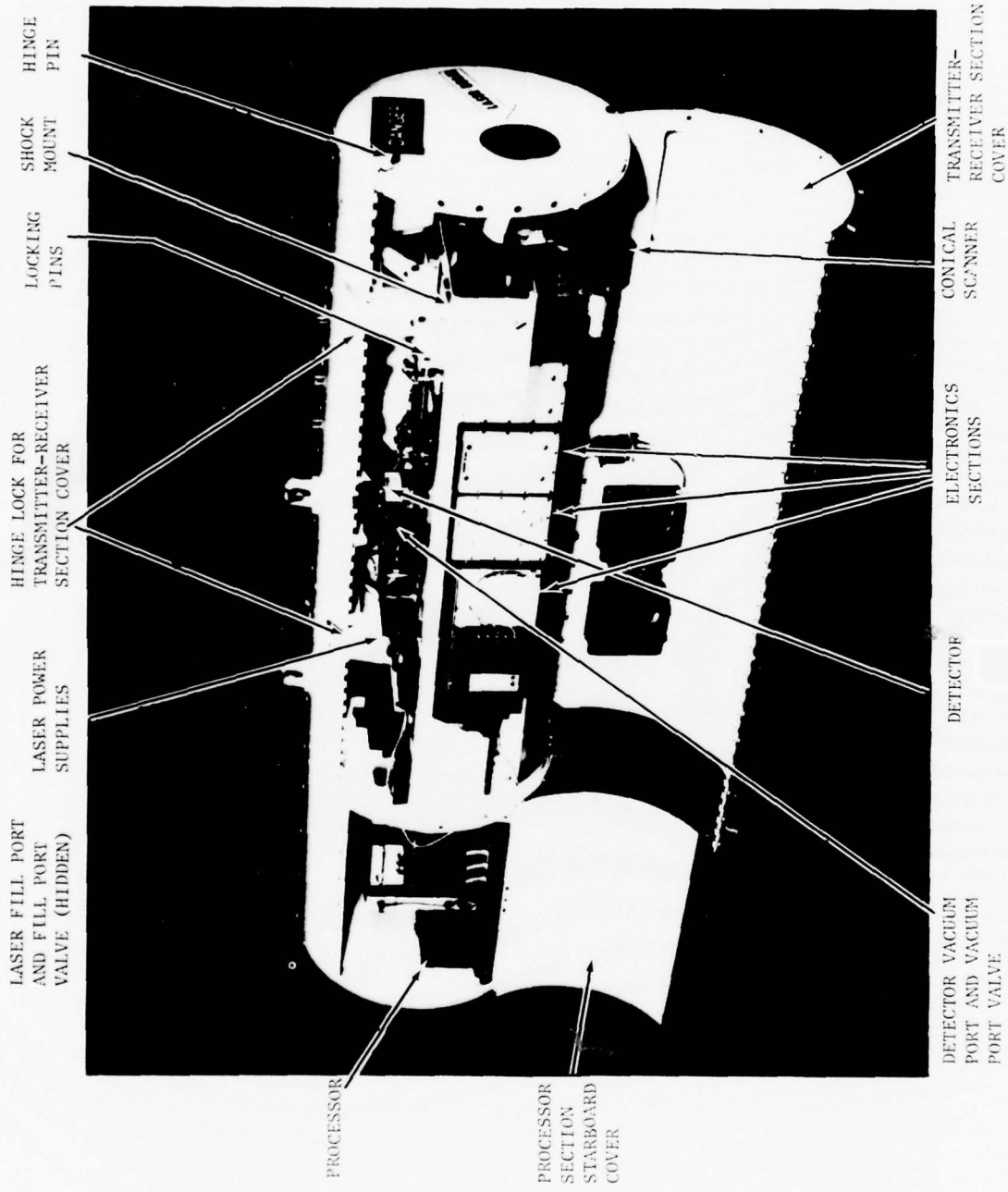


Figure 23. Helicopter carried remote wind sensor with corners open.

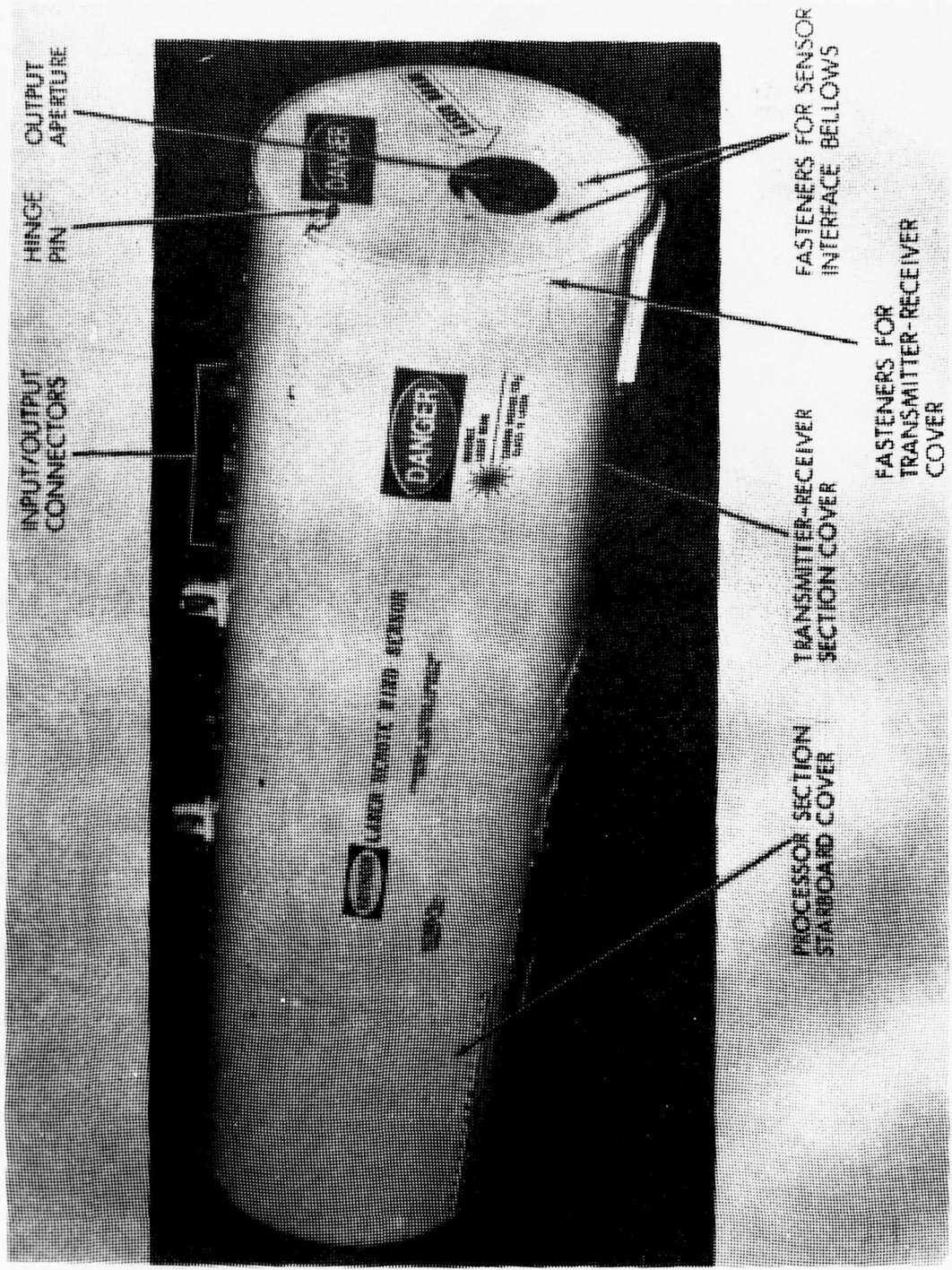


Figure 24. Helicopter carried remote wind sensor.



Figure 25. Mounted helicopter remote wind sensor.



Figure 26. Sensor and tape recorder.

TABLE 1. BEAM EXPANDER SPECIFICATIONS

<u>Input Beam Properties</u>	
Diameter	2.6 mm @ $1/e^2$ points
Shape	Gaussian; TEM ₀₀ mode
Wavelength	10.6 μ m
Power	6 W, CW
Wavefront	Nearly plane wave
<u>Output Beam Properties</u>	
Diameter	66 mm @ $1/e^2$ points at ∞ focus (with no diffraction effects)
Focus	1 to 32 m goal, 2 to 32 m firm
Aberrations	The diameter of the blur circle in which 87% of the total power is contained shall be less than: $\frac{2.6 \lambda R}{D}$ 2 times diffraction limit for Gaussian beam truncated at $1/e^2$ points

where $\lambda = 10.6\mu\text{m}$
 $D = 83 \text{ mm}$
 $R = \text{Range to focus}$

<u>Input Optics</u>	
Clear aperture	5.2 mm
Material	Germanium
Coatings	AR \leq 1/2% per surface
Field angle	On axis
Focal length	Negative

Table 1 (cont)

	<u>Output Optics</u>
Clear aperture	83 mm
Material	Germanium
Coatings	AR \leq 1/2% per surface
Field angle	On axis
Focal length	Positive: effective focal length = 153 mm

Paraxial Magnification

25.4 \times focus range

Surface Reflection Properties

1. The input optics should minimize the back-reflected power onto the detector to less than 50 μ W (see figure 10).
2. The output optics back-reflected power onto the detector should be less than 100 μ W.

TABLE 2. WEDGE SPECIFICATIONS

Total beam deviation	17 deg
Material	Germanium
Clear aperture	83 mm
Closest distance to beam expander output optics	100 mm
Minimum wedge thickness	3 mm
Focus range	1 to 32 m

TABLE 3. MEASURED DETECTOR PARAMETERS

Detector mfg	Honeywell Inc., Radiation Center
Detector type	LK146E9, Mercury Cadmium Telluride (HgCdTe)
Detector serial No.	T-3

Detector Parameter

Quantum efficiency*	42%
Frequency response (-3 dB)*	70 MHz
Maximum LO power	≥ 5 mW
Operating wavelength	P-20 (10.6 μ m)
Dark current**	1.3 mA
Dynamic resistance*	83 Ω
Noise***	-9.8 dB
Series resistance	10.4 Ω
Static resistance*	30.6 Ω

*At operating point of 1 mW LO power with 0.15-V reverse bias and a detector current of 4.9 mA.

**At 0.15-V reverse bias.

***Departure from LO shot noise limited operation. Biased as in * above and at a frequency of 10 MHz.

TABLE 4. TRACKER PARAMETERS

<u>Input</u>	
Frequency coverage (-3 dB)	0.1 to 8.5 MHz
Spectral width	≤ 2 MHz
SNR (1 MHz noise bandwidth)	3 dB
Rate of frequency change	500 MHz/s
Scan rate	20 to 40 Hz
Frequency deviation (P-P)	4 MHz
<u>Discriminator</u>	
Center frequency	60 MHz
Bandwidth	2 MHz
<u>Acquisition</u>	
Acquisition time (max)	255 μ s
VCO sweep rate	50 kHz/ μ s
Samples integrated	30
<u>Tracker</u>	
Time constant	100 μ s
Angle lag (max)	1.5 deg
Frequency lag (@ max df/dt)	50 kHz
<u>Output</u>	
Samples/scan	128
Maximum rate	5120 Hz
LSB	12.5 kHz
Bits	10

TABLE 5. FREQUENCY MEASUREMENTS

Input SNR* (db)	Actual Frequency (MHz)	Measured Frequency	
		Calibrated (MHz)	Uncalibrated (MHz)
15	8.000	8.005	8.048
35	8.000	8.000	8.040
15	1.000	1.0075	1.050
35	1.000	1.0075	1.050
15	0.100	0.1175	0.160
35	0.100	0.1125	0.1475

*Referenced to 1 MHz noise bandwidth

TABLE 6. CONTROLS FOR HRWS

Control	Positions	Function
Laser	On-off	Turn on HV to laser
LVPS	On-off	Turn on low voltage power supplies for control circuits
Sensor	Run	For normal operation
	Pwr	Inserts beam diverter to measure power of transmitter
	No scan	Overrides beam blocking system to permit nonscanning measurements Conical scan switch must be on; RPM adjust at zero
Range	Auto	Performs approximately 1 Hz scan
	Manual	Moves scanner to manually selected range
	Off	Defocuses beam for safety
RPM adjust		Continuously variable RPM from 0 to 1200 for conical scanner
PZT adjust		Adjusts piezoelectric transducer voltage to optimize laser operation
Range adjust		Adjusts position of range scanner; only operational in manual RANGE mode
Conical scan	On-off	Turns on scan motor; CAUTION pre-set RPM adjust to zero
Proc	On-off	Turns on processor
	Cal	Turns on 5 MHz oscillator and turns off input signal
Cal test	Test	Turns on input signal

Table 6 (Cont)

Control	Positions	Function
Cal disable		Disable operation of the self-calibration circuit.
Clock disable	Down	Disconnects 2-deg clock pulse and replaces it with internal clock
Sweep disable	to disable	Disables VCO sweep and sets VCO to 48 MHz
Track disable		Disables acquisition logic so VCO sweeps continuously; pin J3 of the translator can be displayed on an oscilloscope to show the entire spectrum with 2 MHz resolution.
Low air light		Indicates insufficient air flow for laser cooling; the sensor is operable with this light illuminated.
No scan light		Indicates that the no-scan mode is activated and a hazard condition can exist if the transmitted beam is not adequately blocked

Control	Position	Measured Quantity	Units
Monitor selector	I_A, I_B	Laser current	Milliamperes
	Pwr	Laser power	Watts
	V_D	Detector voltage	Volts
	I_D	Detector Current	Milliamperes
	RPM	Scan speed	Revolutions per minute
	Range	Range	See calibration
	-15 V, +15 V, +5 V	Low voltage power supplies	Volts

DISTRIBUTION LIST

Dr. Frank D. Eaton
Geophysical Institute
University of Alaska
Fairbanks, AK 99701

Commander
US Army Aviation Center
ATTN: ATZQ-D-MA
Fort Rucker, AL 36362

Chief, Atmospheric Sciences Div
Code ES-81
NASA
Marshall Space Flight Center,
AL 35812

Commander
US Army Missile R&D Command
ATTN: DRDMI-CGA (B. W. Fowler)
Redstone Arsenal, AL 35809

Redstone Scientific Information Center
ATTN: DRDMI-TBD
US Army Missile R&D Command
Redstone Arsenal, AL 35809

Commander
US Army Missile R&D Command
ATTN: DRDMI-TEM (R. Haraway)
Redstone Arsenal, AL 35809

Commander
US Army Missile R&D Command
ATTN: DRDMI-TRA (Dr. Essenwanger)
Redstone Arsenal, AL 35809

Commander
HQ, Fort Huachuca
ATTN: Tech Ref Div
Fort Huachuca, AZ 85613

Commander
US Army Intelligence Center & School
ATTN: ATSI-CD-MD
Fort Huachuca, AZ 85613

Commander
US Army Yuma Proving Ground
ATTN: Technical Library
Bldg 2100
Yuma, AZ 85364

Naval Weapons Center (Code 3173)
ATTN: Dr. A. Shlanta
China Lake, CA 93555

Sylvania Elec Sys Western Div
ATTN: Technical Reports Library
PO Box 205
Mountain View, CA 94040

Geophysics Officer
PMTC Code 3250
Pacific Missile Test Center
Point Mugu, CA 93042

Commander
Naval Ocean Systems Center (Code 4473)
ATTN: Technical Library
San Diego, CA 92152

Meteorologist in Charge
Kwajalein Missile Range
PO Box 67
APO San Francisco, CA 96555

Director
NOAA/ERL/APCL R31
RB3-Room 567
Boulder, CO 80302

Library-R-51-Tech Reports
NOAA/ERL
320 S. Broadway
Boulder, CO 80302

National Center for Atmos Research
NCAR Library
PO Box 3000
Boulder, CO 80307

R. B. Girardo
Bureau of Reclamation
E&R Center, Code 1220
Denver Federal Center, Bldg 67
Denver, CO 80225

National Weather Service
National Meteorological Center
W321, WWB, Room 201
ATTN: Mr. Quiroz
Washington, DC 20233

Mil Assistant for Atmos Sciences
Ofc of the Undersecretary of Defense
for Rsch & Engr/E&LS - Room 3D129
The Pentagon
Washington, DC 20301

Defense Communications Agency
Technical Library Center
Code 205
Washington, DC 20305

Director
Defense Nuclear Agency
ATTN: Technical Library
Washington, DC 20305

HQDA (DAEN-RDM/Dr. de Percin)
Washington, DC 20314

Director
Naval Research Laboratory
Code 5530
Washington, DC 20375

Commanding Officer
Naval Research Laboratory
Code 2627
Washington, DC 20375

Dr. J. M. MacCallum
Naval Research Laboratory
Code 1409
Washington, DC 20375

The Library of Congress
ATTN: Exchange & Gift Div
Washington, DC 20540
2

Head, Atmos Rsch Section
Div Atmospheric Science
National Science Foundation
1800 G. Street, NW
Washington, DC 20550

CPT Hugh Albers, Exec Sec
Interdept Committee on Atmos Science
National Science Foundation
Washington, DC 20550

Director, Systems R&D Service
Federal Aviation Administration
ATTN: ARD-54
2100 Second Street, SW
Washington, DC 20590

ADTC/DLODL
Eglin AFB, FL 32542

Naval Training Equipment Center
ATTN: Technical Library
Orlando, FL 32813

Det 11, 2WS/OI
ATTN: Maj Orondorff
Patrick AFB, FL 32925

USAFETAC/CB
Scott AFB, IL 62225

HQ, ESD/TOSI/S-22
Hanscom AFB, MA 01731

Air Force Geophysics Laboratory
ATTN: LCB (A. S. Carten, Jr.)
Hanscom AFB, MA 01731

Air Force Geophysics Laboratory
ATTN: LYD
Hanscom AFB, MA 01731

Meteorology Division
AFGL/LY
Hanscom AFB, MA 01731

US Army Liaison Office
MIT-Lincoln Lab, Library A-082
PO Box 73
Lexington, MA 02173

Director
US Army Ballistic Rsch Lab
ATTN: DRDAR-BLB (Dr. G. E. Keller)
Aberdeen Proving Ground, MD 21005

Commander
US Army Ballistic Rsch Lab
ATTN: DRDAR-BLP
Aberdeen Proving Ground, MD 21005

Director
US Army Armament R&D Command
Chemical Systems Laboratory
ATTN: DRDAR-CLJ-I
Aberdeen Proving Ground, MD 21010

Chief CB Detection & Alarms Div
Chemical Systems Laboratory
ATTN: DRDAR-CLC-CR (H. Tannenbaum)
Aberdeen Proving Ground, MD 21010

Commander
Harry Diamond Laboratories
ATTN: DELHD-CO
2800 Powder Mill Road
Adelphi, MD 20783

Commander
ERADCOM
ATTN: DRDEL-AP
2800 Powder Mill Road
Adelphi, MD 20783
2

Commander
ERADCOM
ATTN: DRDEL-CG/DRDEL-DC/DRDEL-CS
2800 Powder Mill Road
Adelphi, MD 20783

Commander
ERADCOM
ATTN: DRDEL-CT
2800 Powder Mill Road
Adelphi, MD 20783

Commander
ERADCOM
ATTN: DRDEL-EA
2800 Powder Mill Road
Adelphi, MD 20783

Commander
ERADCOM
ATTN: DRDEL-PA/DRDEL-ILS/DRDEL-E
2800 Powder Mill Road
Adelphi, MD 20783

Commander
ERADCOM
ATTN: DRDEL-PAO (S. Kimmel)
2800 Powder Mill Road
Adelphi, MD 20783

Chief
Intelligence Materiel Dev & Support Ofc
ATTN: DELEW-WL-I
Bldg 4554
Fort George G. Meade, MD 20755

Acquisitions Section, IRDB-D823
Library & Info Service Div, NOAA
6009 Executive Blvd
Rockville, MD 20852

Naval Surface Weapons Center
White Oak Library
Silver Spring, MD 20910

The Environmental Research
Institute of MI
ATTN: IRIA Library
PO Box 8618
Ann Arbor, MI 48107

Mr. William A. Main
USDA Forest Service
1407 S. Harrison Road
East Lansing, MI 48823

Dr. A. D. Belmont
Research Division
PO Box 1249
Control Data Corp
Minneapolis, MN 55440

Director
Naval Oceanography & Meteorology
NSTL Station
Bay St Louis, MS 39529

Director
US Army Engr Waterways Experiment Sta
ATTN: Library
PO Box 631
Vicksburg, MS 39180

Environmental Protection Agency
Meteorology Laboratory
Research Triangle Park, NC 27711

US Army Research Office
ATTN: DRXRO-PP
PO Box 12211
Research Triangle Park, NC 27709

Commanding Officer
US Army Armament R&D Command
ATTN: DRDAR-TSS Bldg 59
Dover, NJ 07801

Commander
HQ, US Army Avionics R&D Activity
ATTN: DAVAA-0
Fort Monmouth, NJ 07703

Commander/Director
US Army Combat Surveillance & Target
Acquisition Laboratory
ATTN: DELCS-D
Fort Monmouth, NJ 07703

Commander
US Army Electronics R&D Command
ATTN: DELCS-S
Fort Monmouth, NJ 07703

US Army Materiel Systems
Analysis Activity
ATTN: DRXSY-MP
Aberdeen Proving Ground, MD 21005

Director
US Army Electronics Technology &
Devices Laboratory
ATTN: DELET-D
Fort Monmouth, NJ 07703

Commander
US Army Electronic Warfare Laboratory
ATTN: DELEW-D
Fort Monmouth, NJ 07703

Commander
US Army Night Vision &
Electro-Optics Laboratory
ATTN: DELNV-L (Dr. Rudolf Buser)
Fort Monmouth, NJ 07703

Commander
ERADCOM Technical Support Activity
ATTN: DELSD-L
Fort Monmouth, NJ 07703

Project Manager, FIREFINDER
ATTN: DRCPM-FF
Fort Monmouth, NJ 07703

Project Manager, REMBASS
ATTN: DRCPM-RBS
Fort Monmouth, NJ 07703

Commander
US Army Satellite Comm Agency
ATTN: DRCPM-SC-3
Fort Monmouth, NJ 07703

Commander
ERADCOM Scientific Advisor
ATTN: DRDEL-SA
Fort Monmouth, NJ 07703

6585 TG/WE
Holloman AFB, NM 88330

AFWL/WE
Kirtland, AFB, NM 87117

AFWL/Technical Library (SUL)
Kirtland AFB, NM 87117

Commander
US Army Test & Evaluation Command
ATTN: STEWS-AD-L
White Sands Missile Range, NM 88002

Rome Air Development Center
ATTN: Documents Library
TSLD (Bette Smith)
Griffiss AFB, NY 13441

Commander
US Army Tropic Test Center
ATTN: STETC-TD (Info Center)
APO New York 09827

Commandant
US Army Field Artillery School
ATTN: ATSF-CD-R (Mr. Farmer)
Fort Sill, OK 73503

Commandant
US Army Field Artillery School
ATTN: ATSF-CF-R
Fort Sill, OK 73503

Director CFD
US Army Field Artillery School
ATTN: Met Division
Fort Sill, OK 73503

Commandant
US Army Field Artillery School
ATTN: Morris Swett Library
Fort Sill, OK 73503

Commander
US Army Dugway Proving Ground
ATTN: MT-DA-L
Dugway, UT 84022

Dr. C. R. Sreedrahan
Research Associates
Utah State University, UNC 48
Logan, UT 84322

Inge Dirmhirn, Professor
Utah State University, UNC 48
Logan, UT 84322

Defense Documentation Center
ATTN: DDC-TCA
Cameron Station Bldg 5
Alexandria, VA 22314
12

Commanding Officer
US Army Foreign Sci & Tech Center
ATTN: DRXST-IS1
220 7th Street, NE
Charlottesville, VA 22901

Naval Surface Weapons Center
Code G65
Dahlgren, VA 22448

Commander
US Army Night Vision
& Electro-Optics Lab
ATTN: DELNV-D
Fort Belvoir, VA 22060

Commander and Director
US Army Engineer Topographic Lab
ETL-TD-MB
Fort Belvoir, VA 22060

Director
Applied Technology Lab
DAVDL-EU-TSD
ATTN: Technical Library
Fort Eustis, VA 23604

Department of the Air Force
OL-C, 5WW
Fort Monroe, VA 23651

Department of the Air Force
5WW/DN
Langley AFB, VA 23665

Director
Development Center MCDEC
ATTN: Firepower Division
Quantico, VA 22134

US Army Nuclear & Chemical Agency
ATTN: MONA-WE
Springfield, VA 22150

Director
US Army Signals Warfare Laboratory
ATTN: DELSW-OS (Dr. R. Burkhardt)
Vint Hill Farms Station
Warrenton, VA 22186

Commander
US Army Cold Regions Test Center
ATTN: STECR-OP-PM
APO Seattle, WA 98733

Dr. John L. Walsh
Code 5560
Navy Research Lab
Washington, DC 20375

Commander
TRASANA
ATTN: ATAA-PL
(Dolores Anguiano)
White Sands Missile Range, NM 88002

Commander
US Army Dugway Proving Ground
ATTN: STEDP-MT-DA-M (Mr. Paul Carlson)
Dugway, UT 84022

Commander
US Army Dugway Proving Ground
ATTN: STEDP-MT-DA-T
(Mr. William Peterson)
Dugway, UT 84022

Commander
USATRADO
ATTN: ATCD-SIE
Fort Monroe, VA 23651

Commander
USATRADO
ATTN: ATCD-CF
Fort Monroe, VA 23651

Commander
USATRADO
ATTN: Tech Library
Fort Monroe, VA 23651

ATMOSPHERIC SCIENCES RESEARCH PAPERS

1. Lindberg, J.D., "An Improvement to a Method for Measuring the Absorption Coefficient of Atmospheric Dust and other Strongly Absorbing Powders," ECOM-5565, July 1975.
2. Avara, Elton P., "Mesoscale Wind Shears Derived from Thermal Winds," ECOM-5566, July 1975.
3. Gomez, Richard B., and Joseph H. Pierluissi, "Incomplete Gamma Function Approximation for King's Strong-Line Transmittance Model," ECOM-5567, July 1975.
4. Blanco, A.J., and B.F. Engebos, "Ballistic Wind Weighting Functions for Tank Projectiles," ECOM-5568, August 1975.
5. Taylor, Fredrick J., Jack Smith, and Thomas H. Pries, "Crosswind Measurements through Pattern Recognition Techniques," ECOM-5569, July 1975.
6. Walters, D.L., "Crosswind Weighting Functions for Direct-Fire Projectiles," ECOM-5570, August 1975.
7. Duncan, Louis D., "An Improved Algorithm for the Iterated Minimal Information Solution for Remote Sounding of Temperature," ECOM-5571, August 1975.
8. Robbiani, Raymond L., "Tactical Field Demonstration of Mobile Weather Radar Set AN/TPS-41 at Fort Rucker, Alabama," ECOM-5572, August 1975.
9. Miers, B., G. Blackman, D. Langer, and N. Lorimier, "Analysis of SMS/GOES Film Data," ECOM-5573, September 1975.
10. Manquero, Carlos, Louis Duncan, and Rufus Bruce, "An Indication from Satellite Measurements of Atmospheric CO₂ Variability," ECOM-5574, September 1975.
11. Petracca, Carmine, and James D. Lindberg, "Installation and Operation of an Atmospheric Particulate Collector," ECOM-5575, September 1975.
12. Avara, Elton P., and George Alexander, "Empirical Investigation of Three Iterative Methods for Inverting the Radiative Transfer Equation," ECOM-5576, October 1975.
13. Alexander, George D., "A Digital Data Acquisition Interface for the SMS Direct Readout Ground Station - Concept and Preliminary Design," ECOM-5577, October 1975.
14. Cantor, Israel, "Enhancement of Point Source Thermal Radiation Under Clouds in a Nonattenuating Medium," ECOM-5578, October 1975.
15. Norton, Colburn, and Glenn Hoidale, "The Diurnal Variation of Mixing Height by Month over White Sands Missile Range, N.M.," ECOM-5579, November 1975.
16. Avara, Elton P., "On the Spectrum Analysis of Binary Data," ECOM-5580, November 1975.
17. Taylor, Fredrick J., Thomas H. Pries, and Chao-Huan Huang, "Optimal Wind Velocity Estimation," ECOM-5581, December 1975.
18. Avara, Elton P., "Some Effects of Autocorrelated and Cross-Correlated Noise on the Analysis of Variance," ECOM-5582, December 1975.
19. Gillespie, Patti S., R.L. Armstrong, and Kenneth O. White, "The Spectral Characteristics and Atmospheric CO₂ Absorption of the Ho³⁺ YLF Laser at 2.05 μ m," ECOM-5583, December 1975.
20. Novlan, David J. "An Empirical Method of Forecasting Thunderstorms for the White Sands Missile Range," ECOM-5584, February 1976.
21. Avara, Elton P., "Randomization Effects in Hypothesis Testing with Autocorrelated Noise," ECOM-5585, February 1976.
22. Watkins, Wendell R., "Improvements in Long Path Absorption Cell Measurement," ECOM-5586, March 1976.
23. Thomas, Joe, George D. Alexander, and Marvin Dubbin, "SATTEL - An Army Dedicated Meteorological Telemetry System," ECOM-5587, March 1976.
24. Kennedy, Bruce W., and Delbert Bynum, "Army User Test Program for the RDT&E-XM-75 Meteorological Rocket," ECOM-5588, April 1976.

25. Barnett, Kenneth M., "A Description of the Artillery Meteorological Comparisons at White Sands Missile Range, October 1974 - December 1974 ('PASS' - Prototype Artillery [Meteorological] Subsystem)," ECOM-5589, April 1976.
26. Miller, Walter B., "Preliminary Analysis of Fall-of-Shot From Project 'PASS'," ECOM-5590, April 1976.
27. Avara, Elton P., "Error Analysis of Minimum Information and Smith's Direct Methods for Inverting the Radiative Transfer Equation," ECOM-5591, April 1976.
28. Yee, Young P., James D. Horn, and George Alexander, "Synoptic Thermal Wind Calculations from Radiosonde Observations Over the Southwestern United States," ECOM-5592, May 1976.
29. Duncan, Louis D., and Mary Ann Seagraves, "Applications of Empirical Corrections to NOAA-4 VTPR Observations," ECOM-5593, May 1976.
30. Miers, Bruce T., and Steve Weaver, "Applications of Meteorological Satellite Data to Weather Sensitive Army Operations," ECOM-5594, May 1976.
31. Sharenow, Moses, "Redesign and Improvement of Balloon ML-566," ECOM-5595, June, 1976.
32. Hansen, Frank V., "The Depth of the Surface Boundary Layer," ECOM-5596, June 1976.
33. Pinnick, R.G., and E.B. Stenmark, "Response Calculations for a Commercial Light-Scattering Aerosol Counter," ECOM-5597, July 1976.
34. Mason, J., and G.B. Hoidale, "Visibility as an Estimator of Infrared Transmittance," ECOM-5598, July 1976.
35. Bruce, Rufus E., Louis D. Duncan, and Joseph H. Pierluissi, "Experimental Study of the Relationship Between Radiosonde Temperatures and Radiometric-Area Temperatures," ECOM-5599, August 1976.
36. Duncan, Louis D., "Stratospheric Wind Shear Computed from Satellite Thermal Sounder Measurements," ECOM-5800, September 1976.
37. Taylor, F., P. Mohan, P. Joseph and T. Pries, "An All Digital Automated Wind Measurement System," ECOM-5801, September 1976.
38. Bruce, Charles, "Development of Spectrophones for CW and Pulsed Radiation Sources," ECOM-5802, September 1976.
39. Duncan, Louis D., and Mary Ann Seagraves, "Another Method for Estimating Clear Column Radiances," ECOM-5803, October 1976.
40. Blanco, Abel J., and Larry E. Taylor, "Artillery Meteorological Analysis of Project Pass," ECOM-5804, October 1976.
41. Miller, Walter, and Bernard Engebos, "A Mathematical Structure for Refinement of Sound Ranging Estimates," ECOM-5805, November, 1976.
42. Gillespie, James B., and James D. Lindberg, "A Method to Obtain Diffuse Reflectance Measurements from 1.0 to 3.0 μm Using a Cary 17I Spectrophotometer," ECOM-5806, November 1976.
43. Rubio, Roberto, and Robert O. Olsen, "A Study of the Effects of Temperature Variations on Radio Wave Absorption," ECOM-5807, November 1976.
44. Ballard, Harold N., "Temperature Measurements in the Stratosphere from Balloon-Borne Instrument Platforms, 1968-1975," ECOM-5808, December 1976.
45. Monahan, H.H., "An Approach to the Short-Range Prediction of Early Morning Radiation Fog," ECOM-5809, January 1977.
46. Engebos, Bernard Francis, "Introduction to Multiple State Multiple Action Decision Theory and Its Relation to Mixing Structures," ECOM-5810, January 1977.
47. Low, Richard D.H., "Effects of Cloud Particles on Remote Sensing from Space in the 10-Micrometer Infrared Region," ECOM-5811, January 1977.
48. Bonner, Robert S., and R. Newton, "Application of the AN/GVS-5 Laser Rangefinder to Cloud Base Height Measurements," ECOM-5812, February 1977.
49. Rubio, Roberto, "Lidar Detection of Subvisible Reentry Vehicle Erosive Atmospheric Material," ECOM-5813, March 1977.
50. Low, Richard D.H., and J.D. Horn, "Mesoscale Determination of Cloud-Top Height: Problems and Solutions," ECOM-5814, March 1977.

51. Duncan, Louis D., and Mary Ann Seagraves, "Evaluation of the NOAA-4 VTPR Thermal Winds for Nuclear Fallout Predictions," ECOM-5815, March 1977.
52. Randhawa, Jagir S., M. Izquierdo, Carlos McDonald and Zvi Salpeter, "Stratospheric Ozone Density as Measured by a Chemiluminescent Sensor During the Stratcom VI-A Flight," ECOM-5816, April 1977.
53. Rubio, Roberto, and Mike Izquierdo, "Measurements of Net Atmospheric Irradiance in the 0.7- to 2.8-Micrometer Infrared Region," ECOM-5817, May 1977.
54. Ballard, Harold N., Jose M. Serna, and Frank P. Hudson Consultant for Chemical Kinetics, "Calculation of Selected Atmospheric Composition Parameters for the Mid-Latitude, September Stratosphere," ECOM-5818, May 1977.
55. Mitchell, J.D., R.S. Sagar, and R.O. Olsen, "Positive Ions in the Middle Atmosphere During Sunrise Conditions," ECOM-5819, May 1977.
56. White, Kenneth O., Wendell R. Watkins, Stuart A. Schleusener, and Ronald L. Johnson, "Solid-State Laser Wavelength Identification Using a Reference Absorber," ECOM-5820, June 1977.
57. Watkins, Wendell R., and Richard G. Dixon, "Automation of Long-Path Absorption Cell Measurements," ECOM-5821, June 1977.
58. Taylor, S.E., J.M. Davis, and J.B. Mason, "Analysis of Observed Soil Skin Moisture Effects on Reflectance," ECOM-5822, June 1977.
59. Duncan, Louis D. and Mary Ann Seagraves, "Fallout Predictions Computed from Satellite Derived Winds," ECOM-5823, June 1977.
60. Snider, D.E., D.G. Murcray, F.H. Murcray, and W.J. Williams, "Investigation of High-Altitude Enhanced Infrared Background Emissions" (U), SECRET, ECOM-5824, June 1977.
61. Dubbin, Marvin H. and Dennis Hall, "Synchronous Meteorological Satellite Direct Readout Ground System Digital Video Electronics," ECOM-5825, June 1977.
62. Miller, W., and B. Engebos, "A Preliminary Analysis of Two Sound Ranging Algorithms," ECOM-5826, July 1977.
63. Kennedy, Bruce W., and James K. Luers, "Ballistic Sphere Techniques for Measuring Atmospheric Parameters," ECOM-5827, July 1977.
64. Duncan, Louis D., "Zenith Angle Variation of Satellite Thermal Sounder Measurements," ECOM-5828, August 1977.
65. Hansen, Frank V., "The Critical Richardson Number," ECOM-5829, September 1977.
66. Ballard, Harold N., and Frank P. Hudson (Compilers), "Stratospheric Composition Balloon-Borne Experiment," ECOM-5830, October 1977.
67. Barr, William C., and Arnold C. Peterson, "Wind Measuring Accuracy Test of Meteorological Systems," ECOM-5831, November 1977.
68. Ethridge, G.A. and F.V. Hansen, "Atmospheric Diffusion: Similarity Theory and Empirical Derivations for Use in Boundary Layer Diffusion Problems," ECOM-5832, November 1977.
69. Low, Richard D.H., "The Internal Cloud Radiation Field and a Technique for Determining Cloud Blackness," ECOM-5833, December 1977.
70. Watkins, Wendell R., Kenneth O. White, Charles W. Bruce, Donald L. Walters, and James D. Lindberg, "Measurements Required for Prediction of High Energy Laser Transmission," ECOM-5834, December 1977.
71. Rubio, Robert, "Investigation of Abrupt Decreases in Atmospherically Backscattered Laser Energy," ECOM-5835, December 1977.
72. Monahan, H.H. and R.M. Cionco, "An Interpretative Review of Existing Capabilities for Measuring and Forecasting Selected Weather Variables (Emphasizing Remote Means)," ASL-TR-0001, January 1978.
73. Heaps, Melvin G., "The 1979 Solar Eclipse and Validation of D-Region Models," ASL-TR-0002, March 1978.

74. Jennings, S.G., and J.B. Gillespie, "M.I.E. Theory Sensitivity Studies - The Effects of Aerosol Complex Refractive Index and Size Distribution Variations on Extinction and Absorption Coefficients Part II: Analysis of the Computational Results," ASL-TR-0003, March 1978.
75. White, Kenneth O. et al, "Water Vapor Continuum Absorption in the 3.5 μ m to 4.0 μ m Region," ASL-TR-0004, March 1978.
76. Olsen, Robert O., and Bruce W. Kennedy, "ABRES Pretest Atmospheric Measurements," ASL-TR-0005, April 1978.
77. Ballard, Harold N., Jose M. Serna, and Frank P. Hudson, "Calculation of Atmospheric Composition in the High Latitude September Stratosphere," ASL-TR-0006, May 1978.
78. Watkins, Wendell R. et al, "Water Vapor Absorption Coefficients at HF Laser Wavelengths," ASL-TR-0007, May 1978.
79. Hansen, Frank V., "The Growth and Prediction of Nocturnal Inversions," ASL-TR-0008, May 1978.
80. Samuel, Christine, Charles Bruce, and Ralph Brewer, "Spectrophone Analysis of Gas Samples Obtained at Field Site," ASL-TR-0009, June 1978.
81. Pinnick, R.G. et al., "Vertical Structure in Atmospheric Fog and Haze and its Effects on IR Extinction," ASL-TR-0010, July 1978.
82. Low, Richard D.H., Louis D. Duncan, and Richard B. Gomez, "The Microphysical Basis of Fog Optical Characterization," ASL-TR-0011, August 1978.
83. Heaps, Melvin G., "The Effect of a Solar Proton Event on the Minor Neutral Constituents of the Summer Polar Mesosphere," ASL-TR-0012, August 1978.
84. Mason, James B., "Light Attenuation in Falling Snow," ASL-TR-0013, August 1978.
85. Blanco, Abel J., "Long-Range Artillery Sound Ranging: "PASS" Meteorological Application," ASL-TR-0014, September 1978.
86. Heaps, M.G., and F.E. Niles, "Modeling the Ion Chemistry of the D-Region: A case Study Based Upon the 1966 Total Solar Eclipse," ASL-TR-0015, September 1978.
87. Jennings, S.G., and R.G. Pinnick, "Effects of Particulate Complex Refractive Index and Particle Size Distribution Variations on Atmospheric Extinction and Absorption for Visible Through Middle-Infrared Wavelengths," ASL-TR-0016, September 1978.
88. Watkins, Wendell R., Kenneth O. White, Lanny R. Bower, and Brian Z. Sojka, "Pressure Dependence of the Water Vapor Continuum Absorption in the 3.5- to 4.0-Micrometer Region," ASL-TR-0017, September 1978.
89. Miller, W.B., and B.F. Engebos, "Behavior of Four Sound Ranging Techniques in an Idealized Physical Environment," ASL-TR-0018, September 1978.
90. Gomez, Richard G., "Effectiveness Studies of the CBU-88/B Bomb, Cluster, Smoke Weapon" (U), CONFIDENTIAL ASL-TR-0019, September 1978.
91. Miller, August, Richard C. Shirkey, and Mary Ann Seagraves, "Calculation of Thermal Emission from Aerosols Using the Doubling Technique," ASL-TR-0020, November, 1978.
92. Lindberg, James D. et al., "Measured Effects of Battlefield Dust and Smoke on Visible, Infrared, and Millimeter Wavelengths Propagation: A Preliminary Report on Dusty Infrared Test-I (DIRT-I)," ASL-TR-0021, January 1979.
93. Kennedy, Bruce W., Arthur Kinghorn, and B.R. Hixon, "Engineering Flight Tests of Range Meteorological Sounding System Radiosonde," ASL-TR-0022, February 1979.
94. Rubio, Roberto, and Don Hoock, "Microwave Effective Earth Radius Factor Variability at Wiesbaden and Balboa," ASL-TR-0023, February 1979.
95. Low, Richard D.H., "A Theoretical Investigation of Cloud/Fog Optical Properties and Their Spectral Correlations," ASL-TR-0024, February 1979.

96. Pinnick, R.G., and H.J. Auvermann, "Response Characteristics of Knollenberg Light-Scattering Aerosol Counters," ASL-TR-0025, February 1979.
97. Heaps, Melvin G., Robert O. Olsen, and Warren W. Berning, "Solar Eclipse 1979, Atmospheric Sciences Laboratory Program Overview," ASL-TR-0026 February 1979.
98. Blanco, Abel J., "Long-Range Artillery Sound Ranging: 'PASS' GR-8 Sound Ranging Data," ASL-TR-0027, March 1979.
99. Kennedy, Bruce W., and Jose M. Serna, "Meteorological Rocket Network System Reliability," ASL-TR-0028, March 1979.
100. Swingle, Donald M., "Effects of Arrival Time Errors in Weighted Range Equation Solutions for Linear Base Sound Ranging," ASL-TR-0029, April 1979.
101. Umstead, Robert K., Ricardo Pena, and Frank V. Hansen, "KWIK: An Algorithm for Calculating Munition Expenditures for Smoke Screening/Obscuration in Tactical Situations," ASL-TR-0030, April 1979.
102. D'Arcy, Edward M., "Accuracy Validation of the Modified Nike Hercules Radar," ASL-TR-0031, May 1979.
103. Rodriguez, Ruben, "Evaluation of the Passive Remote Crosswind Sensor," ASL-TR-0032, May 1979.
104. Barber, T.L., and R. Rodriguez, "Transit Time Lidar Measurement of Near-Surface Winds in the Atmosphere," ASL-TR-0033, May 1979.
105. Low, Richard D.H., Louis D. Duncan, and Y.Y. Roger R. Hsiao, "Microphysical and Optical Properties of California Coastal Fogs at Fort Ord," ASL-TR-0034, June 1979.
106. Rodriguez, Ruben, and William J. Vechione, "Evaluation of the Saturation Resistant Crosswind Sensor," ASL-TR-0035, July 1979.
107. Ohmstede, William D., "The Dynamics of Material Layers," ASL-TR-0036, July 1979.
108. Pinnick, R.G., S.G. Jennings, Petr Chýlek, and H.J. Auvermann "Relationships between IR Extinction, Absorption, and Liquid Water Content of Fogs," ASL-TR-0037, August 1979.
109. Rodriguez, Ruben, and William J. Vechione, "Performance Evaluation of the Optical Crosswind Profiler," ASL-TR-0038, August 1979.
110. Miers, Bruce T., "Precipitation Estimation Using Satellite Data" ASL-TR-0039, September 1979.
111. Dickson, David H., and Charles M. Sonnenschein, "Helicopter Remote Wind Sensor System Description," ASL-TR-0040, September 1979.